PDX1.1-dependent biosynthesis of vitamin B6 protects roots from ammonium-induced oxidative stress

Ying Liu, Rodolfo A Maniero, Ricardo F.H. Giehl, Michael Melzer, Priscille Steensma, Gabriel Krouk, Teresa B Fitzpatrick, Nicolaus von Wirén

▶ **To cite this version:**

Ying Liu, Rodolfo A Maniero, Ricardo F.H. Giehl, Michael Melzer, Priscille Steensma, et al.. PDX1.1-dependent biosynthesis of vitamin B6 protects roots from ammonium-induced oxidative stress. Molecular Plant, 2022, 15 (5), pp.820-839. 10.1016/j.molp.2022.01.012 . hal-03540746

HAL Id: hal-03540746
https://hal.inrae.fr/hal-03540746

Submitted on 24 Jan 2022

HAL is a multi-disciplinary open access archive for the deposit and dissemination of scientific research documents, whether they are published or not. The documents may come from teaching and research institutions in France or abroad, or from public or private research centers.

L'archive ouverte pluridisciplinaire **HAL**, est destinée au dépôt et à la diffusion de documents scientifiques de niveau recherche, publiés ou non, émanant des établissements d'enseignement et de recherche français ou étrangers, des laboratoires publics ou privés.

Distributed under a Creative Commons Attribution 4.0 International License

Journal Pre-proof

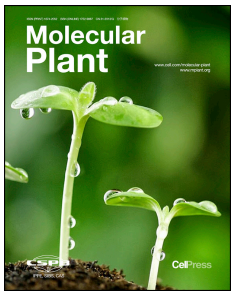

PDX1.1-dependent biosynthesis of vitamin B_6 protects roots from ammonium-induced oxidative stress

Ying Liu, Rodolfo A. Maniero, Ricardo F.H. Giehl, Michael Melzer, Priscille Steensma, Gabriel Krouk, Teresa B. Fitzpatrick, Nicolaus von Wirén

PII: S1674-2052(22)00012-0
DOI: https://doi.org/10.1016/j.molp.2022.01.012
Reference: MOLP 1310

To appear in: *MOLECULAR PLANT*
Accepted Date: 17 January 2022

Please cite this article as: **Liu Y., Maniero R.A., Giehl R.F.H., Melzer M., Steensma P., Krouk G., Fitzpatrick T.B., and von Wirén N.** (2022). PDX1.1-dependent biosynthesis of vitamin B_6 protects roots from ammonium-induced oxidative stress. Mol. Plant. doi: https://doi.org/10.1016/j.molp.2022.01.012.

This is a PDF file of an article that has undergone enhancements after acceptance, such as the addition of a cover page and metadata, and formatting for readability, but it is not yet the definitive version of record. This version will undergo additional copyediting, typesetting and review before it is published in its final form, but we are providing this version to give early visibility of the article. Please note that, during the production process, errors may be discovered which could affect the content, and all legal disclaimers that apply to the journal pertain.

© 2022 The Author

Journal Pre-proof

PDX1.1-dependent biosynthesis of vitamin B_6 protects roots from ammonium-induced oxidative stress

Ying Liu[1], Rodolfo A. Maniero[1], Ricardo F.H. Giehl[1], Michael Melzer[2], Priscille Steensma[3], Gabriel Krouk[4], Teresa B. Fitzpatrick[3], Nicolaus von Wirén[1,*]

[1] Molecular Plant Nutrition, [2]Structural Cell Biology, Leibniz Institute of Plant Genetics and Crop Plant Research (IPK), Corrensstrasse 3, 06466 Gatersleben, Germany

[3] Department of Botany and Plant Biology, University of Geneva, 1211 Geneva, Switzerland

[4] BPMP, Univ Montpellier, CNRS, INRA, SupAgro, Montpellier, France

[*] Corresponding Author: vonwiren@ipk-gatersleben.de

ORCID IDs: 0000-0001-5753-4247 (Y.L.); 0000-0002-1074-8034 (R.A.M.); 0000-0003-1006-3163 (R.F.H.G.); 0000-0002-5213-4030 (M.M.); 0000-0002-3628-2228 (P.S.); 0000-0003-3693-6735 (G.K.); 0000-0001-7694-5631 (T.B.F.); 0000-0002-4966-425X (N.v.W.)

Running title: Vitamin B_6 alleviates ammonium toxicity

Keywords: ammonium nutrition, apoplastic pH, Fe mobilization, root elongation, pyridoxine, ROS scavenging.

SHORT SUMMARY: Ammonium supply triggers a localized Fe-dependent oxidative burst that arrests primary root elongation but also induces PDX1.1-dependent vitamin B_6 production to quench ammonium-induced ROS formation.

ABSTRACT

Despite serving as a major inorganic nitrogen source for plants, ammonium causes toxicity at elevated concentrations, inhibiting root elongation early on. While previous studies have shown that ammonium-inhibited root development relates to ammonium uptake and formation of reactive oxygen species (ROS) in roots, it remained open which mechanisms are underlying the repression of root growth and how plants cope with this inhibitory effect of ammonium. Here, we demonstrate that ammonium-induced apoplastic acidification co-localizes with Fe precipitation and hydrogen

Journal Pre-proof

peroxide (H_2O_2) accumulation along the stele of the elongation and differentiation zone in root tips, indicating Fe-dependent ROS formation. By screening ammonium sensitivity in T-DNA insertion lines of ammonium-responsive genes, we identified *PDX1.1*, which is upregulated by ammonium in the root stele and catalyzes biosynthesis *de novo* of vitamin B_6. Root growth of *pdx1.1* mutants is hypersensitive to ammonium, while chemical complementation or overexpression of *PDX1.1* restores root elongation. This salvage strategy requires non-phosphorylated forms of vitamin B_6 that are able to quench reactive molecular oxygen species and rescue root growth from ammonium inhibition. We propose *PDX1.1*-mediated synthesis of non-phosphorylated B_6 vitamers as a primary strategy to protect roots from ammonium-dependent ROS formation.

Journal Pre-proof

Journal Pre-proof

INTRODUCTION

Nitrogen (N) is an essential mineral element for plant development and extensively applied in crop production (Xu et al., 2012). While synthetic N fertilizers greatly improve global crop yield, the input of nitrate-based N fertilizers also bears environmental risks when leached as nitrate or emitted as nitrogen oxide (Ju et al., 2009; Sutton et al., 2011). Since ammonium is less prone to leaching than nitrate, ammonium-based N fertilizers are widely used nowadays to replace nitrate in agricultural plant production. To increase fertilizer use efficiency, ammonium is often supplied in locally restricted fertilizer strips, where it is present at very high concentrations (Nkebiwe et al., 2016). Although ammonium is a preferential inorganic N source for many plant species (Gazzarrini et al., 1999), excessive ammonium causes toxicity resulting in leaf chlorosis and suppressed root growth (Britto and Kronzucker, 2002). These symptoms rely on ammonium triggering multiple physiological and morphological responses, including changes in apoplastic and cytosolic pH, gene expression, protein modification, ion transport, N metabolism, redox and phytohormone status, as well as root system architecture (Britto and Kronzucker, 2002; Li et al., 2014; Liu and von Wirén, 2017). Against this background and with the increasing use of ammonium-based N fertilizers in agricultural nutrient management, it is important to obtain a deeper understanding of how roots adapt to an ammonium-replete environment.

The most typical morphological changes in root system architecture of ammonium-exposed roots are arrested elongation of primary and lateral roots and enhanced branching of lateral roots (Li et al., 2010; Lima et al., 2010; Liu et al., 2013). Regarding lateral root branching, it has recently been shown that apoplastic acidification caused by AMMONIUM TRANSPORTER (AMT)-mediated ammonium uptake provokes pH-dependent radial auxin diffusion to stimulate locally the emergence of lateral root primordia, forming a highly branched root system (Meier et al., 2020). Given that in several auxin-related mutants root elongation is still as sensitive to ammonium as in wild-type plants, the repression of root elongation by ammonium is unlikely due to altered distribution or action of auxin in plants (Li et al., 2010; Liu et al., 2013). Thus, altered root elongation and lateral root branching under ammonium supply are most likely governed by distinct mechanisms. Neither root elongation nor lateral root branching can be triggered by glutamine, the primary assimilation product of ammonium (Lima et al., 2010; Rogato et al., 2010),

suggesting that ammonium itself or ammonium-related metabolites or signals are critical for root development (Liu and von Wirén, 2017). Indeed, excessive ammonium accumulation and hypersensitive root growth of the *cipk23* mutant indicated that ammonium-induced calcium signaling is required to re-adjust internal NH_4^+/K^+ ratios (Shi et al., 2020). This refers to the function of CIPK23, a CBL-interacting protein kinase, in modulating AMT-, HAK- and AKT-type transporter activities (Ragel et al., 2015; Straub et al., 2017; Sanchez-Barrena et al., 2020; Dong et al., 2021) with strong impact on cytosolic ammonium accumulation and root growth. A further ammonium-related signal may be ethylene, which appears to modulate genes involved in ammonium uptake and assimilation via the transceptor function of NRT1.1 (Jian et al., 2018). Even though these signaling processes help maintaining cytosolic ammonium homeostasis, they do not explain ammonium-dependent root growth inhibition.

Horizontal split agar experiments indicate that the critical region to sense the inhibitory effect of ammonium on root elongation is the root tip (Li et al., 2010). At the cellular level, both cell division and cell elongation are substantially repressed by ammonium, while the integrity of the root stem cell niche remains unaffected (Liu et al., 2013). On the search for mutants overcoming ammonium-induced root growth inhibition, the *vtc1-1* mutant was isolated, which is defective in GMP-mannose pyrophosphorylase (GMPase) and thus not only in downstream ascorbate biosynthesis but also in N-glycosylation of proteins (Qin et al., 2008). However, despite its significant impact on ammonium fluxes (Li et al., 2010), GMPase activity turned out not to be the primary cause of ammonium-dependent root growth inhibition (Kempinski et al., 2011). Transcriptome studies have indicated that enhanced formation of ROS is a typical ammonium-related physiological response (Patterson et al., 2010). Even though significantly higher steady-state H_2O_2 levels in roots were not detected, antioxidative defense systems were induced that comprise ROS-degrading enzymes, including superoxide dismutase, catalase, peroxidase, guaiacol peroxidase and glutathione reductase (Patterson et al., 2010). However, in leaves ammonium toxicity increased H_2O_2 formation, which was found to be mediated by ethylene and followed by enhanced peroxidase activity probably via ABA signaling (Li et al., 2019; Sun et al., 2020). Also in the roots of rice, ammonium treatment increased H_2O_2 contents and induced the heme-heme oxygenase *OsSE5* together with other ROS-detoxifying enzymes including superoxide dismutase, catalase, and ascorbate

peroxidase to relieve ammonium-supplied plants from oxidative stress (Xie et al., 2015). These studies indicate that ammonium toxicity causes ROS formation and that the capacity of enzymatic ROS detoxification is a major determinant of ammonium tolerance in plants. So far, evidence for the involvement of non-enzymatic antioxidants in ammonium-induced oxidative stress defense was not obtained, considering that in roots the pool sizes and oxidative states of NADH, NADPH, glutathione and ascorbate were not substantially altered by ammonium supply (Patterson et al., 2010).

To explore the mechanisms by which ammonium-exposed roots cope with ammonium toxicity and ammonium-dependent ROS formation, we first used a pharmacological approach unraveling localization of the ammonium-triggered H_2O_2 burst. We then screened mutants of ammonium-responsive genes in roots and identified *PDX1.1*, a gene involved in the biosynthesis *de novo* of vitamin B_6. Chemical complementation and genetic approaches showed that non-phosphorylated forms of vitamin B_6 suppressed H_2O_2 formation under ammonium supply. With PDX1.1-dependent vitamin B_6 formation, our study identifies a protective mechanism that spatially overlaps with ammonium-triggered H_2O_2 formation in inner root cells and thus carries potential to better adapt plant roots to ammonium-based fertilization strategies.

RESULTS

Accumulation of H_2O_2 under ammonium supply inhibits primary root elongation

When wild-type seedlings of Arabidopsis were grown on half-strength MS medium for 6 d in the presence of either 1 or 10 mM ammonium as the sole N source, primary root length became 25 or 35% shorter, respectively, than that of nitrate-grown plants (Fig S1A, B). Likewise, total and mean length of lateral roots were repressed to a similar extent as primary root length, suggesting a common mechanism underlying ammonium-induced growth inhibition in both root types (Fig S1B-D). A significant dose-dependent decrease in root elongation rate set in already after 1 d of ammonium exposure suggesting a rapid inhibitory mechanism (Fig S1E-G). Root exposure to ammonium decreased both, cortical cell length and meristem size in a dose-dependent manner and to a similar extent (Fig S1H-J). Since cytokinins determine root meristem size by controlling cell differentiation (Dello Ioio et al. 2007),

we checked the response of cytokinin-sensitive reporter line *TCS:GFP* in the primary root apex, which showed highest expression in the columella and lateral root cap and slight but significant repression under ammonium, revealing that cytokinin signaling was not enhanced by ammonium (Bielach et al., 2012; Fig S2A, B). The histidine kinase AHK3 acts as a cytokinin receptor to stimulate a two-component signaling pathway that transfers a phosphorelay signal to the nucleus, where transcription factors of the type-B ARABIDOPSIS RESPONSE REGULATOR gene family (ARR-B) are activated (Ferreira and Kieber, 2005). We therefore examined ammonium sensitivity via measuring primary root length and meristem size in the *ahk3-3*, *arr1-3* and *arr12-1* mutants, which however revealed no difference to the wild-type (Fig S2C-F), indicating that the AHK3/ARR1 and AHK3/ARR12 two-component cytokinin signaling pathway was not targeted by ammonium. SHY/IAA3 acts directly downstream of ARR1 and ARR12, which increases cell differentiation rate and balances root-meristem size at the transition zone (Dello Ioio et al. 2008). However, neither the *SHY2* deletion line *shy2-31* nor *shy2-2*, which expresses a stabilized proteoform of SHY2 (Tian et al., 2002), exhibited altered ammonium sensitivity of primary root elongation or meristem formation (Fig S2G-J). Taken together, these observations indicated that cytokinin signaling is not involved in ammonium-dependent inhibition of root elongation.

As ammonium has been reported to enhance ROS levels in plants (Patterson *et al.,* 2010; Xie *et al.,* 2015), we stained H_2O_2 in primary roots by 3,3'-diaminobenzidine (DAB). Compared with nitrate, increasing ammonium supply gradually enhanced repression of cell length and meristem size with the detection of H_2O_2 particularly in the elongation and differentiation zones of the root apex (Fig 1A-G). Since nitrate-supplied plants also showed similar DAB staining as ammonium-exposed plants in the meristematic root zone, this zone was not considered as a primary target of ammonium-induced ROS production. To better understand the source of ammonium-dependent ROS formation in primary roots, we employed a pharmacological approach and first applied potassium iodide (KI), acting as a chemical H_2O_2 scavenger (Lee *et al.,* 2013). KI largely reverted the ammonium-dependent inhibition of the primary root elongation rate and restored cell length and meristem size to a large extent (Fig 1A-F). Recovered root elongation coincided with lower abundance of DAB-stained ROS in the elongation and differentiation zone of the primary root

(Fig 1G), suggesting that enhanced levels of H_2O_2 are responsible for the stunted root phenotype. When ammonium-grown roots were exposed to elevated H_2O_2 levels, which were generated either directly by supply of 1 mM H_2O_2 or indirectly by supply of the peroxidase inhibitor salicylhydroxamic acid (SHAM), primary root elongation rates declined drastically due to strongly decreased cell length and meristem size, going along with enhanced DAB staining (Fig S3A-G). Notably, in nitrate-supplied roots, meristem size and DAB staining were apparently not affected by H_2O_2 or SHAM, while cortical cell length was only slightly decreased (Fig S3D-G), relating to the fact that nitrate-supplied plants possess elevated ROS scavenging capacities (Chu et al., 2021). To distinguish between the contribution of superoxide radicals ($O_2^{\bullet-}$) and H_2O_2, we investigated the effects of sodium diethyldithiocarbamate (DDC), an inhibitor of Cu,Zn-superoxide dismutase (SOD) that blocks H_2O_2 generation and leads to $O_2^{\bullet-}$ accumulation (Auh and Murphy, 1995). Both cell length and meristem size of the primary root apex were partially but significantly rescued by DDC supplementation, allowing partial recovery of primary root elongation (Fig S4). This observation indicated that $O_2^{\bullet-}$ radicals are not the direct cause for ammonium-mediated inhibition of root elongation, whereas SOD-catalyzed conversion of $O_2^{\bullet-}$ to H_2O_2 matters. Alternatively, we suspected RBOH-type NADPH oxidases produce ammonium-dependent ROS and examined a couple of *rboh* single or multiple knock-out lines. However, none of them showed an ammonium-dependent root phenotype (Fig S5).

Since in the absence of ammonium H_2O_2 was less effective in inhibiting root elongation (Fig S3), we assumed ammonium-facilitated formation of H_2O_2 plays a role and speculated that this process depends on the availability of Fe (Dixon and Stockwell, 2014). Indeed, lowering Fe supply from 100 µM to 10 µM Fe(III)-EDTA resulted in weaker inhibition of cell length, meristem size and primary root elongation and prevented accumulation of DAB-stained ROS in the elongation and differentiation zone of the primary root (Fig 1A-G). Higher resolution of DAB-stained cells allowed assigning H_2O_2 to the stele of the late elongation and early differentiation zone, which became shorter under increasing ammonium supply and thus appeared more apical (Fig 2A). In addition, we localized ROS-dependent fluorescence by the cell-permeant indicator 2',7'-dichlorofluorescin diacetate (H_2DCFDA), revealing enhanced ROS formation in the stele, especially along the vascular strands of ammonium-exposed roots with a maximum at the transition of the

elongation to the differentiation zone (Fig 2B, C). Considering Fe dependency of ammonium-triggered root inhibition (Fig 1), Fe distribution in the root was stained by DAB-enhanced Perls detecting both free Fe(II) and Fe(III) (Roschzttardtz et al., 2009). While nitrate-grown roots accumulated some Fe in the meristematic zone, ammonium-exposed roots showed much higher Fe accumulation especially in the differentiation zone (Fig 2D). Cross sections of Perls/DAB-stained primary roots showed that ammonium-dependent Fe precipitation was restricted by the Casparian band and thus confined to the apoplast of outer root cells (Fig S6). Since Fe availability increases with decreasing pH and ammonium nutrition is known to acidify the rhizosphere and apoplast (Römheld and Marschner, 1986; Meier et al., 2020), apoplastic pH changes were traced by using the apo-pHusion line, a ratiometric reporter of apoplastic pH (Gjetting et al., 2012). Increasing ammonium nutrition decreased apoplastic pH in particular in the elongation and differentiation zone of ammonium-exposed roots (Fig 2E, F), which co-localized with DAB- or fluorescence-stained ROS (Fig 2A-D), suggesting that the ammonium-dependent pH decrease and enhanced Fe availability caused ROS formation.

Since ammonium-induced repression of root elongation appears to be a rapid response detected even 1 d after ammonium exposure (Fig S1E-G), we investigated dynamic changes in Fe availability and ROS status in ammonium-supplied primary roots. Enhanced Fe precipitation and ROS accumulation appeared as early as 1 d after ammonium supply in the differentiation zone of the primary root and progressed in the apical direction with time and in dependence of external ammonium supply (Fig S7). As indicated by the arrows marking the boundaries of the meristematic and elongation zones, the size of the elongation zone started declining earlier than that of the meristematic zone, which went along with progression of H_2DCFDA-dependent fluorescence into the elongation zone towards the meristematic zone (Fig 2B; S7B). To verify an impact of ROS on cell division, we evaluated the response to ammonium of the cell cycle reporter *CycB1;1::GUS* (Colón-Carmona et al., 1999). Ammonium supply significantly suppressed GUS activity in the apical meristem of primary root, and this suppression was largely alleviated by lowering external Fe supply (Fig S8). Consistent with the decrease of meristem size and cell length under the same conditions (Fig 1D-F), we conclude that Fe-dependent ROS formation is a major repressor of both cell elongation and cell division in ammonium-exposed root apices. Notably, exactly the same responses of apoplastic pH, Fe availability and ROS

Journal Pre-proof

formation as in primary root were detected in the apex of lateral roots (Fig S9), indicating that oxidative stress acts as a common inhibitory mechanism underlying ammonium-induced growth repression in both primary and lateral roots.

To manipulate Fe availability in the presence of ammonium, medium pH was buffered at different values (Fig S10). While ammonium-inhibited root elongation was aggravated when roots were shifted from standard pH 5.7 to pH 5.0, higher pH restored root elongation leading to almost similar length of nitrate- and ammonium-grown roots at pH 7.2 (Fig 3A-C). After 6 d of ammonium exposure, Perls/DAB staining revealed decreasing Fe accumulation in the apical root zone with increasing pH, except for the columella cells (Fig 3D). In contrast, strongly enhanced amounts of Fe accumulated at pH 5.0 but only in ammonium-exposed roots. Since the pH of the agar medium was buffered by MES, we suspected that buffer strength might affect ammonium-induced pH changes and Fe availability under ammonium supply. Indeed, lowering MES concentration from 2.5 to 0.5 mM dramatically aggravated Fe precipitation and inhibition of ammonium-exposed primary root tips, while at 10 mM MES Fe precipitation decreased and ammonium-repressed root elongation was partially attenuated (Fig S11). These results indicated that the intensity of ammonium-dependent proton release and acidification of the rhizosphere is of immediate relevance for Fe mobilization and precipitation in the root apoplast and at the root surface.

The dependence of ammonium-induced root growth inhibition on Fe recalls the role of Fe in root growth inhibition under phosphate deficiency that also relies on Fe-facilitated ROS formation (Müller et al., 2015). Recently, it has been reported that this role of Fe represents a side effect of light exposure when roots are grown in transparent Petri dishes (Zheng et al., 2019). Thus, we shaded the whole root system by aluminium foil as described in Zheng et al. (2019) and noted that in all N treatments primary root length increased when roots were shaded from white light (Fig S12A, B). Even though ammonium-dependent primary root growth inhibition was slightly alleviated by shielding roots from light, ammonium supply still arrested primary root elongation to a large extent (Fig S12B, C). This observation supported that light increases the pool of redox-active Fe (Zheng et al., 2019), which in the presence of ammonium may engage in ROS formation and inhibit primary root elongation.

Previous work under phosphate deficiency showed that blue light exposure promotes the Fenton reaction converting H_2O_2 to hydroxyl radicals that are more toxic oxygen species and strongly suppress primary root elongation (Zheng et al., 2019). Here, to evaluate the involvement of hydroxyl radicals in ammonium-dependent root growth inhibition, we supplied thiourea, a chemical scavenger of hydroxyl radicals (Wasil et al., 1987), together with ammonium to the medium. However, the presence of thiourea hardly altered the sensitivity of primary roots to ammonium (Fig S13), indicating that the formation of hydroxyl radicals via the Fenton reaction is not critical for ammonium-dependent root growth inhibition.

Hypersensitivity of root elongation to ammonium relates to vitamin B_6 deficiency

To explore how plants cope with ammonium-induced H_2O_2 formation and subsequent root growth inhibition, we searched in publicly available transcriptome data for ammonium-responsive genes that are expressed in roots (Patterson *et al.,* 2010; Ristova *et al.,* 2016). We then collected T-DNA insertion lines of 29 ammonium-responsive genes and screened them for primary root length under ammonium versus nitrate supply (Data Set S1). In this screen, we identified a T-DNA insertion line of *PDX1.1* (*SALK_024245*), which was hypersensitive to ammonium treatment (Fig S14A, B). In Arabidopsis, PDX1.1 (along with PDX2) catalyzes vitamin B_6 biosynthesis *de novo* (Tambasco-Studart *et al.,* 2005; Fig S15), thus *pdx1.1* mutants suffer from vitamin B_6 deficiency (Titiz *et al.,* 2006; Wagner *et al.,* 2006; Boycheva *et al.,* 2015). We confirmed the hypersensitive phenotype of *pdx1.1* mutants to ammonium by examining primary root growth in *SALK_024245* and the transposon insertion line *pdx1.1-1* (Figure S14C-E). Since *SALK_024245* and *pdx1.1-1* showed the same growth phenotype under ammonium supply in all our experiments, we focused in the following on *SALK_024245*, naming it *pdx1.1-3*. Given that under nitrate supply primary root growth of *pdx1.1-3* was weaker (Fig 4A), we calculated the relative primary root elongation rate by normalizing it to the root growth rate under nitrate. An earlier and steeper decrease in root elongation rate of *pdx1.1-3* than of the wild type confirmed hypersensitivity of *pdx1.1-3* to ammonium nutrition (Fig 4B, C). The higher sensitivity of *pdx1.1-3* to ammonium went along with elevated accumulation of H_2O_2 in ammonium-exposed primary root tips already 2 d after transfer to ammonium (Fig 4D).

Journal Pre-proof

To confirm whether the hypersensitivity of *pdx1.1-3* to ammonium is due to the defect in vitamin B_6 biosynthesis, we supplied vitamin B_6 in the form of pyridoxine to the growth medium. While external supply of pyridoxine to nitrate-grown wild-type plants had no effect, it largely alleviated ammonium-induced inhibition of primary root growth in the wild type and particularly in the *pdx1.1-3* mutant (Fig 4A). Notably, external supplementation of pyridoxine recovered completely the primary root elongation rate of *pdx1.1-3* (Fig 4B-C), cortical cell length and meristem size (Fig S16) as well as GUS activity of the *CycB1;1::GUS* reporter (Fig S17), confirming that the hypersensitive phenotype of *pdx1.1-3* to ammonium is due to defective vitamin B_6 biosynthesis. Since external supply of pyridoxine reduced also the accumulation of DAB-stained H_2O_2 in ammonium-treated primary roots of both lines (Fig 4E), we conclude that vitamin B_6 alleviates ammonium toxicity either by suppressing H_2O_2 generation or by scavenging H_2O_2 in primary root tips.

Non-phosphorylated forms of vitamin B_6 are critical for ammonium detoxification

Vitamin B_6 is essential for all living organisms, and refers to a group of six different vitamers that contain a pyridine ring and include the non-phosphorylated forms pyridoxal (PL), pyridoxine (PN) and pyridoxamine (PM), as well as the phosphorylated forms pyridoxal 5'-phosphate (PLP), pyridoxine 5'-phosphate (PNP) and pyridoxamine 5'-phosphate (PMP) (Fitzpatrick, 2011; Fig S15). To evaluate their efficacy in mitigating root growth inhibition, we supplied different B_6 vitamers to the medium. Compared with the mock treatment, external supply of PLP slightly retarded the ceasing primary root elongation during the first 4 d after transfer to ammonium, but it hardly restored primary root length after 6 d of ammonium supply (Fig S18A-C). By contrast, exogenous application of the vitamin B_6 forms PL or PN effectively rescued primary root growth under ammonium supply, even during later stages of the treatment, indicating a superior efficacy of the non-phosphorylated B_6 vitamers. When monitoring the H_2O_2 status in root tips in parallel with root elongation, exogenous application of PN or PL but not of PLP quenched excess accumulation of H_2O_2 in ammonium-treated primary root tips (Fig S18D). These results reveal that mitigation of root growth inhibition refers to the non-phosphorylated forms of vitamin B_6 and their ability to suppress H_2O_2 accumulation.

Over-expression of *PDX1.1* improves ammonium tolerance in roots

To address the question whether PDX1.1 plays a role in eliminating ammonium-triggered ROS, we inspected three independent *PDX1.1* overexpression lines (Raschke *et al.,* 2011). All three lines continued elongating their primary roots even after 6 d of ammonium exposure when root elongation of the wild- type was almost completely exhausted (Fig 5A-C). DAB staining showed that overexpression of *PDX1.1* strongly reduced the level of H_2O_2 in ammonium-treated primary roots (Fig 5D). Accordingly, ammonium-induced inhibition of root cortical cell length, meristem size and activity of the *CycB1;1::GUS* reporter also recovered by overexpression of *PDX1.1* (Fig 5E-G; Fig S19), revealing the efficacy of endogenous vitamin B_6 formation under ammonium nutrition. Moreover, an $^{15}NH_4^+$ influx experiment revealed that the ammonium uptake capacity in roots remained unaffected in the *pdx1.1-3* mutant as well as in the *PDX1.1* overexpression lines (Fig 5H). Taken together, elevated expression of *PDX1.1* is sufficient to restore elongation in ammonium-exposed roots and acts downstream of the ammonium uptake process.

Overexpression of *PDX1.1* increases the level of non-phosphorylated B_6 vitamers

As the PDX1-dependent step in vitamin B_6 biosynthesis yields first PLP (Fig S15), we hypothesized that overexpression of *PDX1.1* will primarily increase phosphorylated rather than non-phosphorylated vitamers, whose generation requires an additional phosphatase reaction. Measuring vitamin B_6 in roots confirmed significantly lower levels of total vitamin B_6 in the *pdx1.1-3* mutant than in the wild type, which was caused by a significant decrease in the concentrations of all five determined B_6 vitamers (Fig 6A, B). At first glance, this suggested a constitutive contribution of *PDX1.1* to overall vitamin B_6 biosynthesis because vitamin B_6 levels decreased in *pdx1.1-3* irrespective of the supplied N form. Overexpression of *PDX1.1* led to constitutively higher total vitamin B_6 levels only in *PDX1.1OE-L5*, but under ammonium supply also in *PDX1.1OE-L15* and to lesser extent in *PDX1.1OE-L8*, which coincided with elevated *PDX1.1* transcript levels in these lines (Fig 6A-C). Surprisingly, the concentration of PLP was not enhanced in ammonium-supplied *PDX1.1* overexpression lines, although PLP contributed > 70% to overall vitamin B_6 levels. In contrast, *PDX1.1* overexpression lines showed significantly higher concentrations of non-phosphorylated vitamin B_6 forms than the wild- type, and these

differences closely reflected the relative differences in transcript levels among the three overexpression lines. Hence, the proportion of individual B_6 vitamers shifted towards the non-phosphorylated vitamin B_6 forms, among which PL was the most abundant form contributing up to 25% of total vitamin B_6 (Fig 6B). PM accounted only for approx. 1% of total vitamin B_6 in roots. In wild-type roots, 20% of total vitamin B_6 was in non-phosphorylated forms, while in *pdx1.1-3* this proportion was less than 10%. In *PDX1.1* overexpression lines, between 30% and 40% of total vitamin B_6 was converted into non-phosphorylated forms and this share even increased when plants were grown in the presence of ammonium (Fig 6A, B). We finally correlated the levels of individual B_6 vitamers with those of *PDX1.1* transcripts and revealed close correlations for PN, PL, and PM, but not for PMP, whereas the correlation for PLP was also significant although much weaker (Fig 6D). These results indicate that the extent of *PDX1.1* upregulation by ammonium or by ectopic expression determines primarily the abundance of non-phosphorylated B_6 vitamers without compromising homeostasis of phosphorylated B_6 vitamers in roots.

H_2O_2 triggers localized upregulation of *PDX1.1* under ammonium supply

To investigate the transcriptional regulation of vitamin B_6 biosynthesis and homeostasis by ammonium, the transcript levels of all known genes involved in vitamin B_6 biosynthesis or metabolism were examined by quantitative real-time PCR in roots grown under different N supply. Unexpectedly, *PDX1.1* turned out to be the sole vitamin B_6-related gene that was significantly upregulated by ammonium (Fig 7A). Next, the tissue-specific expression pattern of *PDX1.1* was monitored in plants expressing a *PDX1.1* promoter-GUS reporter construct (Boycheva *et al.,* 2015). *PDX1.1* reporter activity was upregulated by ammonium supply in the root vasculature, increasing from the elongation zone basipetally through the differentiation zone (Fig 7B). As the reporter activity became stronger in the presence of 10 mM ammonium, upregulation of *PDX1.1* expression apparently followed ammonium supply in a dose-dependent manner (Fig 7A, B).

Since the spatial localization of *PDX1.1* expression and H_2O_2 accumulation strongly overlapped in ammonium-treated roots (Fig 2A-B, 7B), the question arose whether ammonium itself or H_2O_2 triggered the upregulation of *PDX1.1*. We thus suppressed H_2O_2 levels in ammonium-exposed roots by supply of KI or by low Fe and observed that *PDX1.1* reporter activity disappeared (Fig 7B). By contrast,

exogenous application of 1 mM H_2O_2 strongly enhanced the promoter activity of *PDX1.1* in the root stele as well as in the apical root meristem, however only in the presence of ammonium (Fig 7C). Therefore, H_2O_2 serves as a signal to upregulate *PDX1.1* transcription upon ammonium nutrition and determine its restricted expression in the stele.

Given that the change of pH upon ammonium exposure is the initial event to trigger the Fe-dependent oxidative burst, we hypothesized that the transcriptional response of *PDX1.1* to ammonium should be influenced by medium pH. Indeed, when *pPDX1.1:GUS* reporter lines were shifted from pH 5.7 to 5.0, the upregulation of *PDX1.1* was enhanced in the presence of ammonium. By contrast, when raising medium pH from 5.7 to 6.5 or 7.2, the induction of *PDX1.1* by ammonium almost disappeared (Fig S20). These findings confirmed that ammonium- and pH-dependent H_2O_2 generation is required to induce the expression of *PDX1.1* in roots.

Elevation of PDX1.1-mediated vitamin B_6 biosynthesis improves tolerance to further nutrient-related stresses

Apart from ammonium toxicity, other nutrient-related stresses also arrest root elongation by elevated ROS formation, such as phosphate deficiency or nickel toxicity (Müller *et al.,* 2015; Zheng *et al.,* 2019; Lesková *et al.,* 2020). We wondered whether PDX1.1-mediated vitamin B_6 biosynthesis also counteracts these oxidative stresses in plants. First, we inspected published transcriptome results (Bhosale et al., 2018; Lesková et al., 2020), to assess the response of vitamin B_6-related genes to phosphate deficiency and nickel toxicity. Surprisingly, none of the known genes involved in vitamin B_6 biosynthesis or metabolism, including *PDX1.1*, was differentially expressed under phosphate deficiency or nickel toxicity (Fig S21A, B). Next, the arrest of primary root elongation under phosphate deficiency or nickel toxicity showed no difference between wild-type (Col-0) and *pdx1.1-3* mutant plants (Fig S21C-F). These results suggested that vitamin B_6-dependent ROS protection did not evolve as a strategy to alleviate oxidative stress in response to phosphate deficiency or nickel toxicity in natural conditions. Nonetheless, coinciding with their enhanced ROS scavenging capacity, all three *PDX1.1* overexpression lines exhibited significantly improved root elongation under phosphate deficiency or nickel toxicity (Fig S21C-F). This result suggests that enhanced *PDX1.1*-mediated vitamin B_6

biosynthesis can be applied as a practical strategy to improve the root tolerance to multiple types of oxidative stress.

DISCUSSION

Application of ammonium-based N fertilizers in agricultural plant production bears the risk of impaired root development when roots are exposed to ammonium-rich soil patches (Britto and Kronzucker, 2002; Watt et al., 2006). Plants have evolved several strategies to cope with the adverse effects of predominant ammonium nutrition, which comprise enhanced N assimilation in roots (Cruz et al., 2005; Guan et al., 2016; Konishi et al., 2017), ammonium compartmentalization to the apoplast or vacuole (Loqué et al., 2005; Li et al., 2010; Bai et al., 2014), and activation of enzymatic antioxidation systems to cope with ammonium-triggered ROS production (Patterson et al., 2010; Xie et al., 2015). In this study, we describe the mechanistic basis underlying ammonium-triggered ROS formation and identify with PDX1.1-dependent vitamin B_6 synthesis a metabolic defense response to counteract ammonium-induced ROS formation.

Ammonium-dependent acidification triggers ROS formation via enhanced Fe mobilization

Ammonium toxicity belongs to one of several mineral element disorders that associate root growth inhibition with the production of ROS (Fig 1; Xie et al., 2015). Among those disorders, localization and generation of ROS differ in an element-specific manner, pointing to different sources of ROS formation. For instance, root growth inhibition by nickel has been related to ROS formation in outer cells of the apical root zone (Leskova et al., 2020), while ROS accumulate predominantly in the meristem and elongation zone under zinc deficiency (Nakayama et al. 2020) or in the root vasculature from the meristematic through the elongation and differentiation zone of salt-stressed plants (Jiang et al., 2012). Considering that experimental visualization and localization of ROS depend not only on the site of generation but also on chemical properties of the ROS-sensitive dye or reporter, we used here DAB staining and H_2DCFDA-dependent fluorescence to localize ROS formation under ammonium nutrition primarily to the vascular cylinder or stele in the elongation and differentiation zones (Fig 2). With increasing ammonium supply and time of exposure ROS formation gradually progressed through the elongation zone towards the

meristem (Fig 2B-C; S7B), where it coincided with suppressed cell length, meristem size and cell division activity (Fig 1; S3; S8), revealing that the apical root meristem is not the primary target of ammonium-dependent ROS generation especially at early stages of ammonium exposure. Although cytokinins are crucial in balancing cell division and meristem size (Dello Ioio et al., 2008), key components of cytokinin signaling are apparently not involved in ammonium-dependent root growth inhibition (Fig S2).

Since ammonium-dependent root growth inhibition was suppressed when H_2O_2 accumulation was chemically quenched by KI (Fig 1) but enhanced when H_2O_2 accumulation was favored in the presence of SHAM or by H_2O_2 supplementation (Fig S3), H_2O_2 or a downstream product must have caused the stunted root phenotype. This is supported by the observation that blocking H_2O_2 formation by DDC in favor of $O_2^{\cdot-}$ accumulation prevented ammonium-dependent root growth inhibition (Fig S4). On the other hand, high effectivity of SOD inhibition by DDC implied that DAB-stained H_2O_2 was generated via $O_2^{\cdot-}$, which in turn may derive from peroxisomes and the mitochondrial electron transport chain or from the activity of NADPH oxidases in the plasma membrane (Smirnoff and Arnaud, 2018). By examining a limited number of available *rboh* single or multiple knock-out lines, we could not find evidence for a role of RBOH-type NADPH oxidases in ammonium-triggered root growth inhibition (Fig S5), even though our assay also included the root stele-localized RBOHF, which triggers vascular ROS formation upon salinity as a prerequisite for salt tolerance (Jiang et al., 2012). Irrespective of the $O_2^{\cdot-}$ source, SOD-mediated dismutation of $O_2^{\cdot-}$ to H_2O_2 consumes protons and is favored by low apoplastic pH (Smirnoff and Arnaud, 2018) that resulted here from ammonium uptake-induced proton secretion (Fig 2; Fig 7D; Meier et al., 2020). Suppressed DAB staining and mitigation of root growth inhibition under low Fe supply (Fig 1) indicated a key role of Fe in H_2O_2 formation. Indeed, exposure of ammonium-grown roots to light, which increases the pool of redox-active Fe (Zheng et al., 2019), aggravated inhibition of root elongation (Fig S12). Furthermore, redox-active Fe(III) likely arose from apoplastic acidification and dissolution of apoplastic Fe pools (Fig S6; Zhu et al., 2018) as well as from UV-dependent photooxidation of EDTA that sets chelated ferric Fe free (Hangarter and Stasinopoulos, 1991). A similarly critical role of ferrous Fe in ROS-mediated root growth inhibition is also known for primary root growth inhibition under phosphate starvation (Müller et al., 2015; Zheng et al., 2019). In this context, exposure of P-

Journal Pre-proof

deficient roots to light favors reduction of ferric to ferrous Fe and subsequent Fe^{2+}-mediated formation of hydroxyl radicals via the Fenton reaction. DAB-stained H_2O_2 under P deficiency is confined to the meristematic root zone and further depends on malate efflux via ALMT1 (Zheng et al., 2019) to increase Fe solubility in the apoplast (Balzergue et al., 2017; Mora-Macías et al., 2017). Since the root elongation in response to ammonium was not altered in *almt1* mutants (Fig S14A, B), root shading restored root elongation only in part (Fig S12) and ammonium-dependent H_2O_2 mainly localized to the root stele above the meristematic zone (Fig 2), mechanisms underlying ROS formation clearly differ between P-deficient and ammonium-exposed roots. Moreover, supplementation of the hydroxyl radical scavenger thiourea, which can restore arrested primary root elongation under P deficiency (Zheng et al., 2019), was poorly effective in the case of ammonium (Fig S13), suggesting that formation of hydroxyl radicals via the Fenton reaction is not critical for ammonium-dependent root growth inhibition. Nonetheless, a determinant role of redox-active Fe in ammonium-triggered root growth inhibition is corroborated by its gradual relief under increasing medium pH, which also decreased Fe accumulation in the root and subsequent Fe availability for ROS metabolism (Fig 3). We thus conclude that ammonium-induced acidification of the root apoplast and additionally in the rhizosphere enhance Fe solubilization as prerequisite for re-location to the stele and subsequent Fe-mediated formation of H_2O_2.

Plant roots counteract ammonium-induced ROS formation via PDX1.1-mediated vitamin B_6 biosynthesis

In plants, vitamin B_6 is synthesized via the “deoxyxylulose-5-phosphate (DXP)-independent pathway”, which utilizes ribose-5-phosphate, glyceraldehyde-3-phosphate and glutamine as substrates for the glutamine amidotransferase complex comprised of pyridoxine synthase (PDX1) and pyridoxine glutaminase (PDX2) (Tambasco-Studart et al., 2005). The primary product is the phosphorylated form PLP (Tambasco-Studart et al., 2005) before enzymes of the salvage pathway facilitate the interconversion among different B_6 vitamers (Colinas et al., 2016; Fig S15). While PLP acts as coenzyme in numerous enzymatic reactions, including those with importance for N assimilation (Percudani and Peracchi, 2003; Fitzpatrick, 2011; Colinas *et al.,* 2016), non-phosphorylated forms of vitamin B_6 serve efficiently as antioxidants *in vitro* and *in vivo* (Bilski et al., 2000; Havaux et al., 2009; Mooney and

Hellmann, 2010). Our study provides several lines of evidence indicating that plants induce PDX1.1-mediated synthesis of non-phosphorylated B_6 vitamers as an efficient strategy to counteract ammonium-dependent oxidative stress in roots.

First, as several enzymes are required for vitamin B_6 biosynthesis and homeostasis, it was surprising that only one of them, *PDX1.1*, responded to ammonium with enhanced expression (Fig 7A). Indeed, overexpression of *PDX1.1* suppressed ammonium-dependent H_2O_2 formation and associated root length inhibition, whereas *pdx1.1* mutant lines were hypersensitive to ammonium (Fig 4 and 5, Fig S14). As in these lines total vitamin B_6 levels closely followed *PDX1.1* transcript levels in roots, transcriptional regulation of PDX1.1-dependent PLP synthesis alone provides sufficient plasticity to counteract the adverse growth effect of ammonium. Among the three paralogs of PDX1 in Arabidopsis, only PDX1.1 and PDX1.3 show catalytic activities (Tambasco-Studart et al., 2005), while *PDX1.2* encodes a pseudoenzyme that can boost vitamin B_6 biosynthesis via heteromerization with its paralogs in response to singlet oxygen or heat stress (Moccand et al., 2014). Although spatial and temporal expression patterns of *PDX1.1* and *PDX1.3* largely overlap and only disruption of both genes causes embryo lethality, PDX1.3 has been found to be more abundant and requisite for stress tolerance than PDX1.1 (Titiz et al., 2006). Nonetheless, enhanced expression of PDX1.3 at the protein level appears to require PDX1.2 (Dell'Aglio *et al.,* 2017), whereas overexpression of PDX1.1 can be achieved with the protein alone to substantially increase vitamin B_6 production (Raschke *et al.,* 2011; Fig 6). This regulatory versatility of PDX1.1 may provide an advantage when plants need to respond instantly to oxidative stresses.

Second, external supply of vitamin B_6 to *pdx1.1-3* mutant or wild-type plants completely prevented ammonium-induced inhibition of root elongation (Fig 4). Although the overall vitamin B_6 level in the *pdx1.1-3* mutant line was only 20-30% lower than in the wild type (Fig 6A), this difference as well as a further 50-100% increase in the overexpressing lines gradually improved root growth, indicating a strong dose dependence of beneficial vitamin B_6 action. This dose-dependent effect went back to the abundance of the non-phosphorylated B_6 vitamers (Fig 6A), because only PL and PN restored root length while the primary biosynthesis product PLP remained ineffective (Fig S18). Superior functionality of non-phosphorylated vitamers as ROS scavengers is most likely determined by substituents of the pyridoxine core that modulate electron density in the ring and thus the interaction with

singlet molecular oxygen ($^1O_2$; Bilski et al., 2000). Upon quenching of $^1O_2$ the pyridoxine ring is degraded (Bilski et al., 2000), explaining the dose-dependent rather than catalytic effect of vitamin B_6 as observed here (Fig 5, 6). Since in overexpression lines root concentrations of the three non-phosphorylated vitamers PM, PN and PL only, correlated closely with *PDX1.1* transcript levels (Fig 6D), transcriptional upregulation of *PDX1.1* is sufficient to confer a B_6 vitamer-specific defense response to stress.

Third, *PDX1.1*-mediated biosynthesis *de novo* of vitamin B_6 spatially and temporally coincides with ammonium-induced ROS formation in roots. Within a time frame of a few days, there was a robust temporal coincidence between root elongation rates and H_2O_2 accumulation, even when vitamin B_6 was provided externally or *PDX1.1* expression levels were modulated (Fig 4, 5). Also at the tissue level, spatial patterns of *PDX1.1* transcript levels and H_2O_2 accumulation strongly overlapped in ammonium-treated roots (Fig 2, 7), supporting the notion that vitamin B_6 biosynthesis is targeted to those tissues and root developmental zones that are most severely affected by ROS accumulation. In plants, biosynthesis *de novo* of vitamin B_6 relies on PDX2 using glutamine as a substrate to produce PLP (Fig S15; Tambasco-Studart et al., 2005; Fitzpatrick et al., 2007; Boycheva et al., 2015). Glutamine is also the most abundant product of ammonium assimilation in roots (Xu et al., 2012; Liu and von Wirén, 2017), which is mediated by cytosolic glutamine synthetase. Interestingly, GLN1;2-mediated glutamine synthesis preferentially localizes in the root vasculature and GLN1;2 represents the most strongly upregulated GLN isoform in ammonium-supplied roots (Ishiyama et al., 2004; Lothier et al., 2011; Guan et al., 2016). Alternatively, ammonium may also be used directly by PDX1.1, independently of PDX2 action, as has been demonstrated *in vitro* (Raschle et al., 2007). In this context, elevated availability not only of glutamine but also of ammonium as one educt for vitamin B_6 synthesis in those cells that suffer most from ROS production may be a factor why plants favored vitamin B_6 as preferential ROS scavenger during evolutionary adaptation to elevated external ammonium levels. Given that ammonium-induced ROS formation occurs in all the cell types of the root differentiation zone and meristem (Fig 2A-C; S7B) while the enhancement of PDX1.1-mediated vitamin B_6 biosynthesis under ammonium supply is confined to the vasculature (Fig 7B; S20), the question arises how root cells that do not produce vitamin B_6 are protected from oxidative stress. Likely there is a radial transport

pathway bringing vitamin B_6 from the vasculature to the outer root cells, driven either by diffusion of non-phosphorylated B_6 vitamers that are considered able to permeate membranes (Stolz and Vielreicher, 2003), or by radial transport via membrane proteins, such as purine permeases (PUPs). In particular PUP1 has been shown to transport non-phosphorylated B_6 vitamers in Arabidopsis as well as after heterologous expression in yeast (Szydlowski et al., 2013).

Vitamin B_6 has proven effective in ROS detoxification in a variety of systems and conditions. In different human cell cultures, the supplementation of non-phosphorylated forms of vitamin B_6 alleviates superoxide-induced damage and lipid peroxidation (Jain and Lim, 2001; Kannan and Jain, 2004; Mahfouz et al., 2009). In Arabidopsis protoplasts, PN supplementation can reduce oxidative damage generated upon high illumination (Danon et al., 2005). When leaf discs were exposed directly to $^1O_2$, lipid peroxidation in the *pdx1.3* background was higher than in the wild type (Havaux et al., 2009). Since this effect was not observed with $O_2^{\cdot -}$ or H_2O_2, and since $^1O_2$ levels rise during illumination more drastically in the *pdx1.3* mutant than in the wild type, vitamin B_6 has been proposed to act as $^1O_2$ quencher (Danon et al., 2005; Havaux et al., 2009). Moreover, $^1O_2$ can easily convert to $O_2^{\cdot -}$ by electron transfer (Khan and Kasha, 1994) and is further converted to H_2O_2 by SOD, allowing reactive Fe to take in a key role in ammonium-induced ROS processing (Fig 7D). Our study could not identify the source of produced $^1O_2$ or $O_2^{\cdot -}$ species, as analysis of a few tested *rboh* mutants did not provide sufficient evidence to rule out NADPH oxidases as a source for $O_2^{\cdot -}$ formation (Fig S5). Alternatively, $^1O_2$ or $O_2^{\cdot -}$ species may derive from electron transport processes in root plastids or mitochondria (Smirnoff and Arnaud, 2018). Irrespective of their origin, their accumulation during repression of SOD by DDC was ineffective in inhibiting root elongation (Fig S4), indicating that the conversion of $O_2^{\cdot -}$ to H_2O_2 by SOD was required to inhibit root elongation (Fig 7D). Actually, these two ROS species greatly influence root development by regulating the balance between cell proliferation and cell differentiation in the root tips (Tsukagoshi, 2016). Specifically, $O_2^{\cdot -}$ localized in the meristematic zone maintains cell division, while H_2O_2 prevailing in the elongation zone stimulates cell differentiation (Tsukagoshi et al., 2010). However, excessive accumulation of H_2O_2 in the elongation zone leads to a repression of root growth reflected by inhibited cell elongation and smaller meristem size (Tsukagoshi et al.,

2010). This may explain how H_2O_2 accumulation inhibited root elongation in ammonium-grown plants (Fig 7D).

Based on our study, we propose a working model of the processes underlying primary root growth inhibition under ammonium nutrition (Fig 7D). Ammonium uptake, which is particularly high in the elongation zone (Duan et al., 2018), provokes apoplastic acidification (Meier et al., 2020) that increases Fe solubilization and re-precipitation in inner root cells (Fig 2, 7D). It is not yet completely clear why Fe preferentially accumulates along the stele and whether the required change in Fe binding forms for xylem loading is involved, but previous studies have confirmed enhanced Fe precipitation in the pericycle and xylem (Green and Rogers, 2004; Roschzttardtz et al., 2013). There, elevated Fe availability and acidic pH favor $O_2^{\bullet-}$ dismutation and H_2O_2 formation (Smirnoff an Arnaud, 2018, Fig 7D). Considering that ammonium uptake-dependent acidification stimulates the generation of H_2O_2, H_2O_2 or a downstream product induces *PDX1.1* expression at the site of Fe and ROS localization (Fig 7B, D). Predominant biosynthesis of non-phosphorylated B_6 vitamers (Fig 6) can subsequently quench reactive molecular oxygen ($^1O_2/O_2^{\bullet-}$) that serves as source for H_2O_2 formation (Fig S4) and thereby counteract ammonium-induced H_2O_2 formation to restore root growth. We find that this PDX1.1-mediated biosynthesis *de novo* of vitamin B_6 is not only essential for protecting roots against ammonium toxicity, as occurring in ammonium-enriched fertilizer bands in agricultural plant production, but also effective against other adverse growth conditions that involve Fe-dependent ROS formation such as P deficiency and nickel toxicity.

MATERIALS AND METHODS

Plant materials and growth conditions

Arabidopsis thaliana accession Col-0 and Ler served as wild type. The following mutants and transgenic lines were used: *ahk3-3* (Dello loio et al., 2007), *arr1-3* (Dello loio et al., 2007), *arr12-1* (Dello loio et al., 2007), *shy2-31* (Dello loio et al., 2008), *shy2-2* (Dello loio et al., 2008), *TCS:GFP* (Bielach et al., 2012), *pdx1.1-1* (Titiz et al., 2006), *pdx1.1-3* (SALK_024245), *apo-pHusion* (Gjetting et al., 2012), *PDX1.1OE-L5* (Raschke et al., 2011), *PDX1.1OE-L8* (Raschke et al., 2011), *PDX1.1OE-L15* (Raschke et al., 2011), *pPDX1.1:GUS* (Boycheva et al., 2015), *CycB1;1::GUS* (Colón-Carmona et al., 1999). The cell cycle reporter *CycB1;1::GUS* (Col-0

background) was introduced into *pdx1.1-3* or *PDX1.1OE-L5* by crossing to generate *CycB1;1::GUS (pdx1.1-3) and CycB1;1::GUS (PDX1.1OE-L5)* lines. Complete information of T-DNA insertion lines of 29 ammonium-responsive genes used in the mutagenesis screen are listed in Data Set S1. Arabidopsis seeds were surface sterilized by 70% ethanol with 0.05% (v/v) Triton X-100, and cultured on modified half-strength Murashige and Skoog (MS) medium containing 100 µM Fe(III)-EDTA, 0.5% sucrose, 1% Duchefa Phyto agar (Duchefa Biochemie), 2.5 mM MES pH 5.7, and N sources were added to different final concentrations as described in the figure legends. Seedlings grown in Petri dishes (12 × 12 cm) were cultured vertically in a growth chamber under a 22°C/18°C and 10/14 h (light/dark) regime at the light intensity of 120 µmol photons m^{-2} s^{-1}. For root phenotyping experiments, plants were pre-cultured on half-strength MS medium containing 1 mM KNO_3 for 6 d, and then transferred to treatment plates supplemented with half-strength MS medium containing 1 mM KNO_3, 1 mM NH_4Cl or 10 mM NH_4Cl respectively. 0.5 mM K_2SO_4 was added to balance K^+ concentration in the ammonium treatment. Root phenotypes were measured 6 d after transfer. To generate P deficiency, 6 days-old plants were transferred to half-strength MS medium containing 625 µM KH_2PO_4 (+P) or 5 µM KH_2PO_4 (-P), KCl was added to -P medium to balance K^+ concentrations. For Ni toxicity, 6 days-old plants were transferred to half-strength MS medium in the absence (-Ni) or presence (+Ni) of 75 µM $NiSO_4$. Root phenotypes were assessed 6 d after transfer. When supplementing H_2O_2, fresh 30% H_2O_2 (Roth) solution (9.79 mol L^{-1}) was diluted to a concentration of 1 M and supplied to the medium after autoclaving. In the root shading experiment, root-containing segments of Petri dishes were covered with aluminium foil as described in Zheng et al. (2019). For vitamin B_6 supplementation experiments, different B_6 vitamers were dissolved in water and supplied to agar medium at a final concentration of 5 µM. Key chemical information is given in Table S1.

Root growth measurements

During root phenotyping experiments, the position of primary roots was labeled every day after treatment in order to calculate primary root elongation rate. Root images were taken by an Epson 10000XL scanner at a resolution of 300 dpi. Primary root growth parameters were measured by WinRHIZO Pro 2007 software (Regents Instruments Canada). Differential interference contrast (DIC) microscopy images of primary root tips were taken to assess the size of primary root meristem and the

length of mature cortical cell as described in Dello Ioio et al. (2007). All the experiments were performed at least twice with similar results.

ROS detection

H_2O_2 in primary root tips were detected by 3,3'-Diaminobenzidine (DAB) staining as described by Thordal-Christensen et al. (1997). Briefly, primary roots were incubated in 1 mg ml^{-1} DAB solution for 8 h, and then imaged by DIC microscopy. H_2O_2 is visualized as a reddish-brown coloration. A cell-permeant fluorogenic dye 2',7'-dichlorodihydrofluorescein diacetate (H_2DCFDA) was also used to measure ROS activity in primary roots. Seedlings were stained for 20 min in a solution of 50 µM H_2DCFDA in 50 mM potassium phosphate buffers (pH 7.0). DCF fluorescence was excited at 488 nm and detected at 517-527 nm. Virtual color images were generated by a rainbow color code to indicate the fluorescence intensity of DCF in roots.

Apoplastic and rhizosphere pH measurements

Apoplastic pH changes were measured by the ratiometric pH reporter apo-pHusion (Gjetting et al., 2012). The fluorescence intensity ratio between pH-sensitive GFP and pH-insensitive RFP was calculated to indicate the changes of apoplastic pH, and virtual ratio images were generated by ImageJ v1.53 software. The changes of rhizosphere pH under different N supply were monitored by the pH indicator bromocresol purple (BCP) that changes color from yellow at pH 5.0 to violet at pH 7.2 (Meier et al., 2020). Six days after growth on different N sources, agar medium containing six seedlings per plate were stained overnight (18 h) with BCP solution at a final concentration of 0.1 mg ml^{-1}.

Histological staining

Promoter-driven β-glucuronidase (GUS) activity was determined by GUS staining as described previously (Li, 2011). Roots were rinsed once with staining buffer containing 50 mM $NaHPO_4$ buffer (pH 7.2), 2 mM potassium ferrocyanide, and 2 mM potassium ferricyanide, and then incubated at 37°C in staining solution containing 2 mM X-Gluc. After staining, roots were cleared by HCG solution (chloral hydrate:water:glycerol = 8:3:1) and imaged by DIC microscopy. To assess the size of the primary root meristem and the length of mature cortical cell, non-staining primary root tips were cleared by HCG solution and imaged by DIC microscopy. To stain Fe accumulation in roots, a Perls staining and DAB/H_2O_2 intensification was performed according to Roschzttardtz et al. (2009). Roots were rinsed three times with 10 mM EDTA, and then incubated for 5 min in a freshly prepared Perls staining solution.

Afterward, roots were incubated in a methanol solution containing 0.01 M NaN_3 and 0.3% (v/v) H_2O_2 for 1 h at room temperature. After washing three times with 0.1 M phosphate buffer (pH 7.4), roots were finally incubated for 5 min in an intensification solution containing 0.025% (w/v) DAB and 0.005% (v/v) H_2O_2 in 0.1 M phosphate buffer (pH 7.4). Roots were mounted with HCG solution before imaging by light microscopy.

Microscopy analyses

Fluorescent images were taken by laser scanning confocal microscopy Zeiss LSM 780. Root samples were stained with 10 µg ml^{-1} propidium iodide (PI) for 5 min to visualize cell walls. GFP was excited at 488 nm and detected at 505-535 nm; RFP was excited at 561 nm and detected at 580-630 nm; PI was excited at 561 nm and detected at 600-700 nm. DCF fluorescence was excited at 488 nm and detected at 517-527 nm. The same microscope settings were kept to measure all confocal sections across samples. Fluorescence quantification of apo-pHusion and H_2DCFDA were conducted by Zeiss ZEN microscope software (version 2.6). Virtual ratio images were generated by Image J 1.53 software. DAB staining, Perls staining, GUS staining and DIC images were taken by Zeiss Axio Imager 2 system. For light microscopy of *in situ*-localized Fe, root cuttings of 5 mm length of 5 seedlings from each growth condition, were dissected approximately 1 cm above the root tip and subjected to aldehyde fixation, dehydration and resin embedding as described in Table S2. Semi-thin sections of 2.5 µm thickness were cut with a Leica UCT microtome (Leica Microsystems, Wetzlar, Germany), and mounted on slides in rapid mounting medium Entelan (Sigma-Aldrich, Darmstadt, Germany). Sections were recorded with a 40x lense at fixed exposure time using a Zeiss Axio Imager M2 (Carl Zeiss Microscopy GmbH, Oberkochen, Germany).

Vitamin B_6 quantification analysis

The abundance of all individual B_6 vitamers in roots were determined by HPLC. Vitamin B_6 quantification analyses were performed as described previously (Colinas et al., 2016) with the following changes: two separate extractions were performed with 15 volumes and 8 volumes of 50 mM ammonium acetate (pH 4.0), respectively, and a 50 µL injection volume was used for a single run per extract.

Real-time quantitative PCR

Total RNA was extracted from 10-20 mg frozen root samples by RNeasy plant mini kit (Qiagen) following the manufacturer's protocol. Template cDNA was synthesized from 1 µg total RNA using SuperScript II Reverse Transcriptase (Thermo Fisher Scientific) and Oligo d(T)12-18 primer. Real-time qPCR was performed by CFX384 Touch Real-Time PCR Detection System (Bio-Rad) using iQ SYBR Green Supermix (Bio-Rad). According to the multiple internal control method (Vandesompele et al., 2002), relative transcript levels of target genes were calculated by the geNorm algorithm (https://genorm.cmgg.be), using *UBQ10 (AT4G05320)* and *ACTIN2 (AT3G18780)* as the multiple internal control genes in this study. Gene specific primers for qPCR are listed in Table S3.

Statistical analysis

Data were collected and analyzed by Microsoft Excel 2016. Statistical analyses were conducted by Graphpad Prism 8 (version 8.3.0). Two-tailed Student's *t*-test, Dunnett's multiple test or Tukey's HSD test was performed to test the statistical significance, and the *P*-value of each statistical analysis is described in the figure legends. Graphs were plotted by Graphpad Prism 8 (version 8.3.0), and edited by Adobe Illustrator 2020 (version 24.2.1).

Accession numbers

Sequence data in this study can be found in the Arabidopsis Information Resource (TAIR) according to the following accession numbers: *PDX1.1 (AT2G38230), PDX1.2 (AT3G16050), PDX1.3 (AT5G01410), PDX2 (AT5G60540), PDX3 (AT5G49970), SOS4 (AT5G37850), PLR1 (AT5G53580), UBQ10 (AT4G05320)* and *ACTIN2 (AT3G18780)*.

AUTHOR CONTRIBUTIONS

Y.L. and N. v. W. conceived the project and designed the experiments. Y.L., R.F.H.G., R.A.M., M.M., P.S. and T.B.F. performed the experiments and analyzed the data. G.K. provided the transcriptome data. Y.L. and N.v.W. wrote the manuscript with support of R.F.H.G. and T.B.F.

ACKNOWLEDGMENTS

We thank Twan Rutten (IPK Gatersleben) for microscopy advice. We thank Markus Meier, Cevza Esin Tunc, and Mohammad-Reza Hajirezaei (IPK Gatersleben) for scientific advice and valuable discussions. We further thank Jacqueline Fuge, Annett

Bieber, Elis Fraust, Barbara Kettig, Yudelsy Antonia Tandron Moya, Dagmar Böhmert and Christine Bethmann (IPK Gatersleben) for excellent technical assistance. This work was supported by the Deutsche Forschungsgemeinschaft (DFG, Germany) with a grant (WI1728/13-2) to N.v.W. The Swiss National Science Foundation is also acknowledged for funding to T.B.F. (grants 31003A_14117 and IZLIZ3_183193).

FIGURE LEGENDS

Figure 1. Involvement of H_2O_2 and Fe in ammonium-dependent root growth inhibition.

(A) Root phenotype of wild-type plants 6 d after transfer to different N supply, which contained additionally either 0.5 mM potassium iodide (KI) or 10 µM Fe(III)-EDTA (low Fe) instead of 100 µM Fe(III)-EDTA as in control plates. Horizontal marks along the root axis indicate daily positions of primary root tips. Root images were scanned 6 d after transfer. Scale bar = 1 cm. **(B)** - **(C)** Relative primary root elongation rate under 1 mM ammonium supply **(B)** or under 10 mM ammonium supply **(C)**, normalized to the growth rate of plants treated with 1 mM nitrate. Symbols represent means ± SE, n = 20 plants per treatment. Asterisks denote significant differences between control and indicated treatments at each time point as * P<0.05 ** P<0.01 *** P<0.001 according to Dunnett's multiple test. **(D)** Cell length and meristem size of primary roots. The length of mature cortical cells and the size of the root apical meristem are indicated by yellow arrowheads. DIC images of primary root tips were taken at 6 d after transfer. Scale bar = 100 µm. **(E)** - **(F)** Quantitative readout of mature cortical cell length **(E),** and primary root meristem size **(F)**. Boxes show the first quartile, median and third quartile; the whiskers show the minimum and maximum values, n = 16 plants. Different letters represent significant differences between treatments according to two-way ANOVA followed by Tukey's HSD test, P<0.05. **(G)** DAB staining of H_2O_2 in primary root tips at 6 d after treatment. The reddish-brown coloration indicates H_2O_2. Representative images from 10 plants per treatment are shown. Scale bar = 200 µm.

Figure 2. Ammonium-dependent histochemical changes in the primary root apex.

(A) DAB staining of H_2O_2 in primary root tips at 6 d after treatment. The reddish-brown coloration indicates H_2O_2. Representative images from 10 plants per treatment are shown. Scale bar = 100 µm. **(B)** Staining of ROS (oxidant levels) by H_2DCFDA

staining. Rainbow color code (black to white) indicates DCF fluorescence intensity (low to high). Scale bars: 100 µm. **(C)** Quantitative readout of the fluorescence intensity of H_2DCFDA staining in different zones of the primary root. The boxes show the first quartile, median and third quartile; the whiskers show the minimum and maximum values. n = 10 independent plants. Different letters represent significant differences within each individual root zone at $P<0.05$ according to Tukey's HSD test. **(D)** Perls/DAB staining of Fe as indicated by a reddish-brown color. Scale bars: 100 µm. **(E)** Activity of the apoplastic pH sensor apo-pHusion. Color code (black to white) indicates fluorescence intensity ratio of eGFP/mRFP1 (low to high) and thus apoplastic pH. Scale bars: 100 µm. **(F)** Quantitative readout of the intensity ratio of eGFP/mRFP in different developmental zones of the primary root. Boxes show the first quartile, median and third quartile; the whiskers show the minimum and maximum values; n = 10 independent plants. Different letters represent significant differences within each individual root zone at $P<0.05$ according to Tukey's HSD test. After a pre-culture of 6 d, wild-type or apo-pHusion plants were transferred to the treatment medium supplied with differing N forms. Histological staining and fluorescent imaging were performed 6 d after treatment. Representative images from 10 plants per treatment are shown. Yellow arrowheads in **(A)** and **(D)**, or white arrowheads in **(B)** and **(E)**, indicate the boundaries of the meristematic zone, elongation zone and differentiation zone along the primary root.

Figure 3. Influence of medium pH on primary root growth and root tissue Fe.

(A) Root phenotype of wild-type plants 6 d after transfer to different N supply buffered at different pH. Medium pH of 5.0, 5.7 and 6.5 was buffered by 2.5 mM MES, while pH 7.2 was buffered by 2.5 mM MOPS. Horizontal marks along the root axis indicate daily positions of primary root tips. Scale bar = 1 cm. **(B)** - **(C)** Relative primary root elongation rate under 1 mM ammonium supply **(B)** or under 10 mM ammonium supply **(C)**, normalized to the growth rate of plants treated with 1 mM nitrate. Symbols represent means ± SE, n = 20 plants per treatment. Asterisks denote significant differences between control (pH 5.7) and indicated treatments at each time point as * $P<0.05$ ** $P<0.01$ *** $P<0.001$ according to Dunnett's multiple test. **(D)** Perls/DAB staining of Fe as indicated by a reddish-brown color. Perls/DAB staining was conducted at 6 d after transfer. Representative images from 10 plants per treatment are shown. Scale bars: 100 µm.

Figure 4. Exogenous application of vitamin B_6 alleviates ammonium toxicity in roots.

(A) Root phenotype of Col-0 and *pdx1.1-3* mutant plants 6 d after transfer to different N supply in the absence or presence of 5 µM vitamin B_6 (pyridoxine). Horizontal marks along the root axis indicate daily positions of primary root tips. Scale bar = 1 cm. **(B)** - **(C)** Relative primary root elongation rate under 1 mM ammonium supply **(B)** or under 10 mM ammonium supply **(C)**, normalized to the growth rate of plants treated with 1 mM nitrate. Data represent means ± SE, n = 20 plants per treatment. Different letters represent significant differences at each time point at $P<0.05$ according to Tukey's HSD test. **(D)** H_2O_2 accumulation in the primary root as visualized by DAB staining in wild-type and *pdx1.1-3* mutant plants under differing N supply. DAB staining was conducted 2 d after treatment (2DAT) or 6 d after treatment (6DAT). Representative images from 10 seedlings per treatment are shown. Scale bar = 200 µm. **(E)** DAB staining of H_2O_2 in primary root tips 6 d after treatment. The reddish-brown coloration indicates H_2O_2. Representative images from 10 seedlings per treatment are shown. Scale bar = 200 µm.

Figure 5. Over-expression of *PDX1.1* enhances ammonium tolerance in roots.

(A) Root phenotype of wild-type, *pdx1.1-3* mutant and three independent *PDX1.1* overexpression lines subjected to different N supply. Horizontal marks along the root axis indicate daily positions of primary root tips. After pre-culture of 6 d, plants were transferred to media containing different N forms. Root images were taken at 6 days after transfer. Scale bar = 1 cm. **(B)** - **(C)** Relative primary root elongation rate under 1 mM ammonium supply **(B)** or under 10 mM ammonium supply **(C)**, normalized to the growth rate of plants treated with 1 mM nitrate. Symbols represent means ± SE, n = 20 plants per treatment. Asterisks denote significant differences between wild type and indicated lines at each time point as * $P<0.05$ ** $P<0.01$ *** $P<0.001$ by Dunnett's multiple test. **(D)** DAB staining of H_2O_2 in primary root tips of wild type, *pdx1.1-3* and *PDX1.1OE-L5* at 6 d after treatment. The reddish-brown coloration indicates H_2O_2. Representative images from 10 plants per treatment are shown. Scale bar = 200 µm. **(E)** Cell length and meristem size of primary roots of wild type, *pdx1.1-3* and *PDX1.1OE-L5*. The length of mature cortical cells and the size of the root apical meristem are indicated by yellow arrowheads. DIC images of primary root tips were taken 6 d after treatment. Scale bar = 100 µm. **(F)** - **(G)** Quantitative readout of mature cortical cell length **(F)**, and primary root meristem size **(G)**. Boxes show the

first quartile, median and third quartile; the whiskers show the minimum and maximum values, n = 16 plants. Different letters represent significant differences between lines and treatments according to two-way ANOVA followed by Tukey's HSD test, $P<0.05$. **(H)** Influx of $^{15}NH_4^+$ into roots of wild type, *pdx1.1-3* mutant and *PDX1.1* overexpression lines. Plants were pre-cultured hydroponically for 5 weeks and then subjected to N starvation for 4 d before being transferred to 200 µM ^{15}N-labeled NH_4^+ for 6 min. Bars represent means ± SD, n = 5 biological replicates. Asterisks denote significant differences between wild type and indicated lines at * $P<0.05$ by Dunnett's multiple test; ns = not significant.

Figure 6. Vitamin B_6 profiling of *pdx1.1* mutant and *PDX1.1*-overexpressing plants under different N regimes.

(A) Root concentrations of vitamin B_6, pyridoxamine 5'-phosphate (PMP), pyridoxal 5'-phosphate (PLP), pyridoxamine (PM), pyridoxine (PN) and pyridoxal (PL) in wild type (Col-0), *pdx1.1-3* mutant and three *PDX1.1* overexpression lines 6 d after transfer to different N supply. The amount of pyridoxine 5'-phosphate (PNP) was too low to be detected in this study. Bars represent means ± SD, n = 4 independent biological replicates. Asterisks denote significant differences between wild type and indicated lines at * $P<0.05$ ** $P<0.01$ *** $P<0.001$, by Dunnett's multiple test; ND = not detected. **(B)** Proportion of individual B_6 vitamers in the roots and **(C)** relative transcript abundance of *PDX1.1* in the roots of wild type, *pdx1.1-3* and *PDX1.1* overexpression lines 6 d after transfer to different N supplies. The relative transcript level of *PDX1.1* was determined by quantitative real-time PCR, and normalized by using *ACTIN2* and *UBQ10* as internal controls. Bars represent means ± SD, n = 4 independent biological replicates. **(D)** Correlation between the transcript abundance of *PDX1.1* and the concentration of individual B_6 vitamers in roots of wild type, *pdx1.1-3* and *PDX1.1* overexpression lines. Pearson's correlation coefficients are shown as R values.

Figure 7. Transcriptional regulation of *PDX1.1* and other vitamin B_6-related genes in response to ammonium.

(A) Relative transcript abundance of *PDX1.1, PDX1.2, PDX1.3, PDX2, PDX3, SOS4* and *PLR1* in roots of wild-type plants 6 d after transfer to different N supplies. Relative transcript levels were determined by quantitative real-time PCR and normalized by using both *ACTIN2* and *UBQ10* as multiple internal controls. Bars represent means ± SD, n = 3 biological replicates. Different letters represent

963 significant differences among means at $P<0.05$ according to Tukey's HSD test, ns =
964 not significant. **(B)** - **(C)** Promoter activity of the *pPDX1.1:GUS* reporter in primary
965 roots 6 d after transfer to different N treatments in the absence or presence of 0.5
966 mM KI or under supply of 10 µM Fe(III)-EDTA (low Fe) **(B)** or in the presence of 1
967 mM H_2O_2 **(C)**. Representative images from 10 plants per treatment are shown. Scale
968 bar = 100 µm. **(D)** Working model for the role of ammonium-triggered proton release
969 in Fe-dependent ROS metabolism and subsequent vitamin B6 formation. Ammonium
970 uptake provokes proton secretion and apoplastic acidification which increases Fe
971 solubilization in the root apoplast and the rhizosphere along the elongation and
972 differentiation zones of the root. Secreted protons i) mobilize Fe from ETDA or the
973 apoplastic Fe pool ($Fe(OH)_3$), ii) enable superoxide dismutase (SOD)-mediated
974 conversion of superoxide ($O_2^{\cdot-}$) to H_2O_2. H_2O_2 upregulates *PDX1.1* expression to
975 enhance accumulation of non-phosphorylated B_6 vitamers, in particular pyridoxine
976 (PN) and pyridoxal (PL), which serve as antioxidants quenching the reactive
977 molecular oxygen species $^1O_2$ or $O_2^{\cdot-}$. The root images on the right and left side refer
978 to the primary root tips of DAB-stained seedlings and *pPDX1.1:GUS* reporter lines
979 under ammonium supply, respectively.
980
981

Journal Pre-proof

SUPPLEMENTAL FIGURE LEGENDS

Figure S1. Ammonium suppresses root elongation in Arabidopsis.

(A) Visual appearance of seedlings subjected to different N supplies. Wild-type plants were pre-cultured on half-strength MS medium containing 1 mM NO_3^- for 6 d before being transferred to 1 mM NO_3^-, 1 mM NH_4^+ or 10 mM NH_4^+ as sole N source. During plant growth, the positions of primary root tips were labeled every day to calculate primary root elongation rates. Images were taken 6 d after transfer. Scale bar = 1 cm. **(B)** - **(D),** Primary root length **(B)**, total lateral root length **(C)**, and mean lateral root length **(D)** of wild-type plants 6 d after transfer to different N treatments. Boxes show the first quartile, median and third quartile; the whiskers show the minimum and maximum values, n = 20 independent plants. Different letters represent significant differences at $P<0.05$ according to Tukey's HSD test. **(E) - (G),** Primary root length **(E)**, primary root elongation rate **(F)**, and relative primary root elongation rate **(G)** of wild-type plants under differing N supplies. Symbols represent means ± SE, n = 20 plants per treatment. Different letters in **(E)** and **(F)** represent significant differences within each time point at $P<0.05$ according to Tukey's HSD test. Different letters in **(G)** denote significant differences among time points under 1 mM or 10 mM NH_4^+ respectively, according to Tukey's HSD test. **(H)** Cell length and meristem size of primary roots. Primary roots were stained by propidium iodide (PI), and confocal images were taken 6 d after transfer. The length of mature cortical cells and the size of the root apical meristem are indicated by red arrowheads. Scale bar = 100 µm. **(I) - (J),** Quantitative readout of primary root meristem size **(I)**, and mature cortical cell length **(J)**. Boxes show the first quartile, median and third quartile; the whiskers show the minimum and maximum values, n = 20 plants. Different letters represent significant differences at $P<0.05$ according to Tukey's HSD test.

Figure S2. Cytokinin signaling is not involved in ammonium-dependent inhibition of root growth.

(A) Expression pattern of the cytokinin reporter *TCS:GFP* in primary root tips under different N supply. Images were taken 6 d after transfer. **(B)** Quantitative readout of *TCS:GFP* fluorescence intensity in primary roots under different N supply. Boxes show the first quartile, median and third quartile; the whiskers show minimum and maximum values, n = 10 plants. Asterisks denote significant differences between wild type and indicated lines at * $P<0.05$ by two-tailed Student's *t*-test. **(C)** and **(G)**, Root phenotype of wild-type (Col-0), *ahk3-3, arr1-3, arr12-1* mutants **(C)**, and wild-type

(Ler), *shy2-31*, *shy2-2* mutants **(G)** subjected to different N supply. Roots were scanned at 6 d after transfer. Scale bar = 1 cm. The position of primary root tips at the day of transfer is labeled by black arrowheads. **(D)** and **(H)**, Primary root length after transfer of Col-0, *ahk3-3, arr1-3, arr12-1* **(D)**, and Ler, *shy2-31*, *shy2-2* **(H)** to different N supply. Boxes show the first quartile, median and third quartile; the whiskers show the minimum and maximum values, n = 10 plants in **(D)**, n = 12 plants in **(H)**. Different letters represent significant differences between treatments and lines according to two-way ANOVA followed by Tukey's HSD test at $P<0.05$. **(E)** and **(I)**, Primary root meristems of Col-0, *ahk3-3, arr1-3, arr12-1* **(E)**, and Ler, *shy2-31*, *shy2-2* **(I)** under different N supply. The size of the primary root meristem is indicated by yellow arrowheads in the images. Root images were taken at 6 d after transfer to indicated N sources. Scale bar = 100 µm. **(F)** and **(J)**, Quantitative readout of the primary root meristem size of Col-0, *ahk3-3, arr1-3, arr12-1* **(F)**, and Ler, *shy2-31*, *shy2-2* **(J)**. Boxes show the first quartile, median and third quartile; the whiskers show the minimum and maximum values, n = 10 plants in **(F)**, n = 12 plants in **(J)**. Different letters represent significant differences between treatments and lines according to two-way ANOVA followed by Tukey's HSD test at $P<0.05$.

Figure S3. H_2O_2 aggravates root growth inhibition in the presence of ammonium.

(A) Root phenotype of wild-type plants 6 d after transfer to different N supply, in the absence or presence of either 1 mM H_2O_2 or 20 µM SHAM. Horizontal marks along the root axis indicate daily positions of primary root tips. Root images were scanned 6 d after transfer. Scale bar = 1 cm. **(B)** - **(C)** Relative primary root elongation rate under 1 mM ammonium supply **(B)** and under 10 mM ammonium supply **(C)**, normalized to the growth rate of plants treated with 1 mM nitrate. Symbols represent means ± SE, n = 20 plants per treatment. Asterisks denote significant differences between control and indicated treatments at each time point as * $P<0.05$ ** $P<0.01$ *** $P<0.001$ according to Dunnett's multiple test. **(D)** Cell length and meristem size of primary roots. The length of mature cortical cells and the size of the root apical meristem are indicated by yellow arrowheads. DIC images of primary root tips were taken at 6 d after transfer. Scale bar = 100 µm. **(E)** - **(F)** Quantitative readout of cortical cell length **(E)**, and meristem size **(F)**. Boxes show the first quartile, median and third quartile; the whiskers show the minimum and maximum values, n = 16 plants. Different letters represent significant differences between samples according

to two-way ANOVA followed by Tukey's HSD test at $P<0.05$. **(G)** DAB staining of H_2O_2 in primary root tips at 6 d after treatment. The reddish-brown coloration indicates H_2O_2. Representative images from 10 plants per treatment are shown. Scale bar = 200 µm.

Figure S4. Superoxide is not causal for ammonium-dependent root growth inhibition.

(A) Schematic diagram of ROS metabolism and inhibitor action. Sodium diethyldithiocarbamate (DDC) acts as an inhibitor of superoxide dismutase (SOD), potassium iodide (KI) acts as H_2O_2 scavenger, and salicylhydroxamic acid (SHAM) is a peroxidase inhibitor (Lee *et al.,* 2013). **(B)** Root phenotype of wild-type plants 6 d after transfer to different N supply in the absence or presence of 100 µM DDC. Horizontal marks along the root axis indicate daily positions of primary root tips. Scale bar = 1 cm. **(C)** - **(D)** Relative primary root elongation rate under 1 mM ammonium supply **(C)** and under 10 mM ammonium supply **(D)**, normalized to the growth rate of plants treated with 1 mM nitrate. Symbols represent means ± SE, n = 20 plants per treatment. Asterisks denote significant differences between control and DDC treatment at each time point according to two-tailed Student's *t*-test at *** $P<0.001$. **(E)** Cell length and meristem size of primary roots. Primary roots were stained by propidium iodide, and confocal images were taken 6 d after transfer. The length of mature cortical cells and the size of the root apical meristem are indicated by red arrowheads. Scale bar = 100 µm. **(F) - (G)** Quantitative readout of cortical cell length **(F)**, and meristem size **(G)**. Boxes show the first quartile, median and third quartile; the whiskers show the minimum and maximum values, n = 20 plants. Different letters represent significant differences between samples according to two-way ANOVA followed by Tukey's HSD test at $P<0.05$.

Figure S5. Screening of *rboh* mutants under different N supply.

(A) Root phenotypes of wild-type plants and single or multiple *rboh* mutants in response to different N supply. After a pre-culture of 6 d, seedlings were transferred to medium containing either 1 mM nitrate or 1 mM ammonium as sole N source. Horizontal marks along the root axis indicate daily positions of primary root tips. Images were taken 6 d after treatment. Scale bar = 1 cm. **(B)** Primary root length after transfer. Boxes show the first quartile, median and third quartile; the whiskers show the minimum and maximum values, n = 18 plants. Different letters represent

significant differences between samples according to two-way ANOVA followed by Tukey's HSD test at $P<0.05$.

Figure S6. Fe precipitation in the primary root under nitrate or ammonium supply.

After a pre-culture of 6 d, wild-type plants were transferred to the medium supplied with 1 mM nitrate, 1 mM ammonium or 10 mM ammonium. Perls/DAB stained roots were embedded in Spurr resin. Root cross-sections were obtained from the differentiation zone of primary roots. Fe precipitation in primary roots is indicated by a reddish-brown colour. Scale bars: 50 µm.

Figure S7. Dynamic changes of the Fe and ROS status in primary root tips under different N supply.

(A) Perls/DAB staining of Fe as indicated by a reddish-brown color. After a pre-culture of 6 d, wild type (Col-0) plants were transferred to the treatment medium supplied with differing N forms. Histological staining was performed at the indicated days after transfer (DAT). Scale bars: 100 µm. **(B)** ROS status (oxidant levels) in primary root tips as monitored by H_2DCFDA staining. DCF fluorescence was detected by confocal microscopy at the indicated time points. Rainbow color code (black to white) indicates DCF fluorescence intensity (low to high). Scale bars: 100 µm. **(C)** Quantitative readout of the fluorescence intensity of H_2DCFDA staining. The boxes show the first quartile, median and third quartile; the whiskers show the minimum and maximum values, n = 12 plants. Different letters represent significant differences between samples at $P<0.05$ according to Tukey's HSD test. Orange arrowheads in **(A)**, or white arrowheads in **(B)**, indicate the boundaries of the meristematic zone, elongation zone and differentiation zone along the primary root.

Figure S8. Fe aggravates ammonium-repressed cell division in roots.

(A) GUS activity in primary root tips of a *CycB1;1::GUS* reporter line. After a pre-culture of 6 d, *CycB1;1::GUS* reporter plants were transferred to treatment medium supplied with different N forms. The treatment medium contained 100 µM Fe(III)-EDTA (control) or 10 µM Fe(III)-EDTA (low Fe). Histological staining was performed 6 d after transfer. Scale bar = 100 µm. **(B)** Quantitative readout of the dividing cell number in primary root tips of *CycB1;1::GUS* reporter line. Boxes show the first quartile, median and third quartile; the whiskers show the minimum and maximum values, n = 12 plants. Different letters represent significant differences between samples according to two-way ANOVA followed by Tukey's HSD test at $P<0.05$.

Figure S9. Ammonium-dependent histochemical changes in the lateral root apex.

(A) Cell length and meristem size of lateral root. After a pre-culture of 6 d, wild type (Col-0) seedlings were transferred to the treatment medium supplied with different N forms. Six days after transfer, lateral roots were stained by propidium iodide and imaged by confocal microscopy. The length of mature cortical cells and the size of the meristem are indicated by red arrowheads. Scale bar = 100 µm. **(B)** - **(C)**, Quantitative readout of lateral root meristem size **(B)**, and lateral root cortical cell length **(C)**. Boxes show the first quartile, median and third quartile; the whiskers show the minimum and maximum values, n = 20 plants. Different letters represent significant differences at $P<0.05$ according to Tukey's HSD test. **(D)** DAB staining of H_2O_2 in lateral root tips at 6 d after treatment. The reddish-brown coloration indicates H_2O_2. Representative images from 10 plants per treatment are shown. Scale bar = 100 µm. **(E)** Detection of ROS (oxidant levels) by H_2DCFDA staining. Rainbow color code (black to white) indicates DCF fluorescence intensity (low to high). Scale bars: 100 µm. **(F)** Quantitative readout of the fluorescence intensity of H_2DCFDA staining in lateral roots. The boxes show the first quartile, median and third quartile; the whiskers show the minimum and maximum values. n = 12 plants. Different letters represent significant differences at $P<0.05$ according to Tukey's HSD test. **(G)** Perls/DAB staining of Fe in lateral root tips as indicated by a reddish-brown color. Representative images from 10 plants per treatment are shown. Scale bars: 100 µm. **(H)** Activity of the apoplastic pH sensor apo-pHusion in lateral roots. Color code (black to white) indicates fluorescence intensity ratio of eGFP/mRFP1 (low to high) and thus apoplastic pH. Scale bars: 100 µm. **(I)** Quantitative readout of the intensity ratio of eGFP/mRFP in lateral root. Boxes show the first quartile, median and third quartile; the whiskers show the minimum and maximum values; n = 12 plants. Different letters represent significant differences at $P<0.05$ according to Tukey's HSD test. Yellow arrowheads in **(D)** and **(G)**, or white arrowheads in **(E)** and **(H)**, indicate the boundaries of the meristematic and elongation zone along the lateral root.

Figure S10. Changes in rhizosphere pH after supply of different N forms.

After a pre-culture of 6 d, wild-type (Col-0) seedlings were transferred to the treatment medium supplied with different N forms. Medium pH of 5.0, 5.7 and 6.5 was buffered by 2.5 mM MES, while pH 7.2 was buffered by 2.5 mM MOPS. Changes of medium pH through plants are monitored by the pH indicator

bromocresol purple (BCP) that changes color from yellow at pH 5.0 to violet at pH 7.2, while the left side of the plates without plants serves as a blank.

Figure S11. Influence of buffer strength on root growth and root Fe status.

(A) Root phenotype of wild-type (Col-0) plants 6 d after transfer to treatment medium containing MES buffer at different strength. Horizontal marks along the root axis indicate daily positions of primary root tips. Scale bar = 1 cm. **(B)** - **(C)** Relative primary root elongation rate under supply of 1 mM ammonium **(B)** or 10 mM ammonium **(C)**, normalized to the growth rate of plants treated with 1 mM nitrate. Symbols represent means ± SE, n = 20 plants per treatment. Asterisks denote significant differences between 2.5 mM MES and indicated treatments at each time point as * P<0.05 ** P<0.01 *** P<0.001 according to Dunnett's multiple test. **(D)** Perls/DAB staining of Fe in primary root tips as indicated by a reddish-brown color. Perls/DAB staining was conducted at 6 d after transfer. Representative images from 10 plants per treatment are shown. Scale bars: 100 µm.

Figure S12. Light is not essential for ammonium-dependent inhibition of primary root elongation.

(A) Experimental setup of the root shading treatment. Petri dish-grown plants were exposed to white light in the control treatment (light), while the whole root zone was covered by aluminium foil in the shading treatment (shading), as described in Zheng et al. (2019). **(B)** Appearance of plants grown on the indicated nitrogen supply. After a pre-culture of 6 d, wild-type (Col-0) plants were transferred to the treatment plates and either exposed to light or shaded. Images were taken 6 d after transfer. Scale bar = 1 cm. **(C)** Primary root length after transfer of wild-type plants to light or shading. Boxes show the first quartile, median and third quartile; the whiskers show minimum and maximum values; n = 20 plants. Different letters represent significant differences at P<0.05 according to Tukey's HSD test.

Figure S13. The formation of hydroxyl radicals is not critical for ammonium-inhibited root elongation.

(A) Root phenotype of wild-type (Col-0) plants 6 d after transfer to different N supplies in the absence (control) or presence of 0.5 mM or 1.0 mM thiourea. Horizontal marks along the root axis indicate daily positions of primary root tips. Scale bar = 1 cm. **(B)** - **(C)** Relative primary root elongation rate under supply of 1 mM ammonium **(B)** or 10 mM ammonium **(C)**, normalized to the growth rate of plants treated with 1 mM nitrate. Symbols represent means ± SE, n = 20 plants per treatment. Asterisks denote significant differences between control and thiourea

treatments at each time point as * P<0.05 ** P<0.01 *** P<0.001 according to Dunnett's multiple test.

Figure S14. *pdx1.1* mutants are hypersensitive to ammonium.

(A) Phenotypic screening of T-DNA insertion lines of ammonium-responsive genes. Primary root length under ammonium supply was taken as a read-out for ammonium sensitivity. Candidate lines were pre-cultured on half-strength MS medium containing 1 mM nitrate for 6 d before being transferred to medium containing either 1 mM nitrate or 1 mM ammonium as sole N source. Horizontal marks along the root axis indicate daily positions of primary root tips. Images were taken 6 d after transfer. Scale bar = 1 cm. **(B)** Relative primary root length after transfer to 1 mM ammonium, normalized to the root length of plants treated with 1 mM nitrate. Asterisks denote significant differences between wild-type (Col-0) and indicated lines as *** P<0.001 according to by Dunnett's multiple test; ns = not significant. **(C)** Schematic diagram of the T-DNA insertions in the *PDX1.1* gene. Positioning of the T-DNA insertion in *pdx1.1-3 (SALK_024245)* and the transposon insertion in *pdx1.1-1 (SM_3_22664)* (Titiz *et al.,* 2006). **(D)** Root phenotype of wild-type (Col-0), *pdx1.1-1* and *pdx1.1-3* plants subjected to different N supplies. Horizontal marks along the root axis indicate daily positions of primary root tips. Images were taken 6 d after transfer. Scale bar = 1 cm. **(E)** Primary root length of wild-type (Col-0) and *pdx1.1* mutant plants after transfer to different N forms. Boxes show the first quartile, median and third quartile; the whiskers show minimum and maximum values; n = 18 plants. Different letters represent significant differences between samples according to two-way ANOVA followed by Tukey's HSD test, P<0.05.

Figure S15. Vitamin B_6 metabolism in Arabidopsis.

Vitamin B_6 comprises six different vitamers. PLP, as a phosphorylated B_6 vitamer is a bioactive form participating as coenzyme in numerous enzymatic reactions. Non-phosphorylated forms of vitamin B_6 are PN, PL, and PM. In plants, PLP is produced by biosynthesis *de novo* (blue) or by the salvage pathway (brown) via the conversion among different B_6 vitamers. This schematic is modified from Colinas et al. (2016). Gln, glutamine; Glu, glutamate; R5P, ribose 5-phosphate; G3P, glyceraldehyde 3-phosphate; PNP, pyridoxine 5'-phosphate; PLP, pyridoxal 5'-phosphate; PMP, pyridoxamine 5'-phosphate; PN, pyridoxine; PL, pyridoxal; PM, pyridoxamine; P-ase, phosphatase.

Figure S16. Exogenous application of vitamin B_6 rescues cell length and meristem size under ammonium supply.

(A) - **(B)** Cell length and meristem size of primary roots of wild-type (Col-0) **(A)** or *pdx1.1-3* mutant **(B).** Plants grown under different N supply and in the absence (- VB_6) or presence (+ VB_6) of 5 µM pyridoxine. DIC images of primary roots were taken 6 d after transfer. The length of mature cortical cells and the size of the root apical meristem are indicated by yellow arrowheads. Scale bar = 100 µm. **(C)** - **(D)** Quantitative readout of cortical cell length **(C)**, and meristem size **(D)**. Boxes show the first quartile, median and third quartile; the whiskers show the minimum and maximum values, n = 16 plants. Different letters represent significant differences between samples according to three-way ANOVA followed by Tukey's HSD test, $P<0.05$.

Figure S17. Exogenous application of vitamin B_6 restores cell division under ammonium supply.

(A) GUS activity of the *CycB1;1::GUS* reporter in primary roots of wild-type (Col-0) and *pdx1.1-3* mutant plants. After a pre-culture of 6 d, *CycB1;1::GUS* reporter lines were transferred to different N forms in the absence (- VB_6) or presence (+ VB_6) of 5 µM pyridoxine. Histological staining were performed 6 d after treatment. Scale bar = 100 µm. **(B)** Quantitative readout of the number of dividing cells. Boxes show the first quartile, median and third quartile; the whiskers show the minimum and maximum values, n = 12 plants. Different letters represent significant differences among treatments according to three-way ANOVA followed by Tukey's HSD test at $P<0.05$.

Figure S18. Non-phosphorylated forms of vitamin B_6 are critical for ammonium detoxification.

(A) Root phenotype of wild-type (Col-0) plants 6 d after transfer to different N supply in the absence or presence of 5 µM vitamin B_6 provided either as pyridoxal 5'-phosphate (PLP), pyridoxal (PL), or pyridoxine (PN). Horizontal marks along the root axis indicate daily positions of primary root tips. Seedlings subjected to N supplies with exogenous supplementation of different B_6 vitamers. Scale bar = 1 cm. **(B)** - **(C)** Relative primary root elongation rate under 1 mM ammonium supply **(B)** or under 10 mM ammonium supply **(C)**, normalized to the growth rate of plants treated with 1 mM nitrate. Symbols represent means ± SE, n = 20 plants per treatment. Asterisks denote significant differences between control and indicated treatments at each time point as * $P<0.05$ ** $P<0.01$ *** $P<0.001$ according to Dunnett's multiple test. **(D)** DAB staining of H_2O_2 in primary root tips 6 d after treatment. The reddish-brown coloration

indicates H_2O_2. Representative images from 10 seedlings per treatment are shown. Scale bar = 200 µm.

Figure S19. Over-expression of *PDX1.1* rescues cell division under ammonium supply.

(A) GUS activity of the *CycB1;1::GUS* reporter in primary root tips of wild-type (Col-0), *pdx1.1-3* and *PDX1.1OE-L5* plants. After a pre-culture of 6 d, *CycB1;1::GUS* reporter lines were transferred to the treatment medium supplied with different N forms. Histological stainings were performed 6 d after transfer. Scale bar = 100 µm. **(B)** Quantitative readout of the number of dividing cells in primary root tips of *CycB1;1::GUS* reporter lines. Boxes show the first quartile, median and third quartile; the whiskers show the minimum and maximum values, n = 12 plants. Different letters represent significant differences between treatments and lines according to two-way ANOVA followed by Tukey's HSD test at $P<0.05$.

Figure S20. Influence of medium pH on the expression of *PDX1.1* upon ammonium supply.

Promoter activities of the *pPDX1.1:GUS* reporter in primary roots subjected to different N forms and buffered at different pH were monitored by GUS staining 6 d after transfer. Medium pH of 5.0, 5.7 and 6.5 was buffered by 2.5 mM MES, while pH 7.2 was buffered by 2.5 mM MOPS. Representative images from 10 plants per treatment are shown. Scale bar = 100 µm.

Figure S21. Over-expression of *PDX1.1* improves tolerance to P deficiency and Ni toxicity.

(A) - **(B)** Heat map displaying the relative expression level of vitamin B_6-related genes (highlighted in boxes) in response to phosphorus deficiency **(A)** or nickel toxicity **(B)**. Data were retrieved from published microarray experiments (Bhosale et al., 2018; Lesková et al., 2020). Selected genes previously shown to be up- or down-regulated by phosphorus deficiency or nickel toxicity were included as controls. -P, 5 µM phosphate; +P, 625 µM phosphate; ++Ni, 100 µM nickel; control, no nickel added to growth medium. **(C)** Appearance of plants grown on different phosphate (P) supplies. After a pre-culture of 6 d, the seedlings of Col-0, *pdx1.1-3*, *PDX1.1OE-L5*, *PDX1.1OE-L15* and *PDX1.1OE-L8* were transferred to treatment medium containing 625 µM P (+P) or 5 µM P (-P). Images were taken 6 d after transfer. Scale bar = 1 cm. **(D)** Primary root length after transfer. Root phenotyping of indicated lines was conducted 6 d after transfer. Boxes show the first quartile, median and third quartile;

the whiskers show minimum and maximum values; n = 20 plants. Different letters represent significant differences between treatments and lines according to two-way ANOVA followed by Tukey's HSD test at $P<0.05$. **(E)** Appearance of plants subjected to nickel (Ni) toxicity. After a pre-culture of 6 d, the seedlings of wild-type (Col-0), *pdx1.1-3*, *PDX1.1OE-L5*, *PDX1.1OE-L15* and *PDX1.1OE-L8* were transferred to half-strength MS medium in the absence (- Ni) or presence (+ Ni) of 75 µM Ni. Images were taken 6 d after transfer. Scale bar = 1 cm. **(F)** Primary root length after transfer. Root phenotypes were recorded 6 d after transfer. Boxes show the first quartile, median and third quartile; the whiskers show minimum and maximum values; n = 20 plants. Different letters represent significant differences between samples according to two-way ANOVA followed by Tukey's HSD test at $P<0.05$.

Table S1. Chemical Information.

Table S2. Protocol for fixation, dehydration and embedding of root tissue.

Table S3. Primers used in this study.

Data Set S1. Information on ammonium-responsive genes used for the mutant screening in this study.

Journal Pre-proof

REFERENCES

Auh, C.K., and Murphy, T.M. (1995). Plasma-membrane redox enzyme is involved in the synthesis of O_2^- and H_2O_2 by phytophthora elicitor-stimulated rose cells. Plant Physiol 107:1241-1247.

Bai, L., Ma, X., Zhang, G., Song, S., Zhou, Y., Gao, L., Miao, Y., and Song, C.P. (2014). A receptor-like kinase mediates ammonium homeostasis and is important for the polar growth of root hairs in Arabidopsis. Plant Cell 26:1497-1511.

Balzergue, C., Dartevelle, T., Godon, C., Laugier, E., Meisrimler, C., Teulon, J.M., Creff, A., Bissler, M., Brouchoud, C., Hagege, A., et al. (2017). Low phosphate activates STOP1-ALMT1 to rapidly inhibit root cell elongation. Nat Commun 8:15300.

Bhosale, R., Giri, J., Pandey, B.K., Giehl, R.F.H., Hartmann, A., Traini, R., Truskina, J., Leftley, N., Hanlon, M., Swarup, K., et al. (2018). A mechanistic framework for auxin dependent Arabidopsis root hair elongation to low external phosphate. Nat Commun 9:1409.

Bielach, A., Podlesakova, K., Marhavy, P., Duclercq, J., Cuesta, C., Muller, B., Grunewald, W., Tarkowski, P., and Benkova, E. (2012). Spatiotemporal regulation of lateral root organogenesis in Arabidopsis by cytokinin. Plant Cell 24:3967-3981.

Bilski, P., Li, M.Y., Ehrenshaft, M., Daub, M.E., and Chignell, C.F. (2000). Vitamin B6 (pyridoxine) and its derivatives are efficient singlet oxygen quenchers and potential fungal antioxidants. Photochem Photobiol 71:129-134.

Boycheva, S., Dominguez, A., Rolcik, J., Boller, T., and Fitzpatrick, T.B. (2015). Consequences of a deficit in vitamin B6 biosynthesis de novo for hormone homeostasis and root development in Arabidopsis. Plant Physiol 167:102-117.

Britto, D.T., and Kronzucker, H.J. (2002). NH_4^+ toxicity in higher plants: a critical review. J Plant Physiol 159:567-584.

Buettner, G.R., Doherty, T.P., and Patterson, L.K. (1983). The kinetics of the reaction of superoxide radical with Fe(III) complexes of EDTA, DETAPAC and HEDTA. Febs Lett 158:143-146.

Chu, X., Wang, J.G., Li, M., Zhang, S., Gao, Y., Fan, M., Han, C., Xiang, F., Li, G., Wang, Y., et al. (2021). HBI transcription factor-mediated ROS homeostasis regulates nitrate signal transduction. Plant Cell 33:3004-3021.

Coleto, I., Bejarano, I., Marin-Pena, A.J., Medina, J., Rioja, C., Burow, M., and Marino, D. (2021). *Arabidopsis thaliana* transcription factors MYB28 and MYB29 shape ammonium stress responses by regulating Fe homeostasis. New Phytol 229:1021-1035.

Colinas, M., Eisenhut, M., Tohge, T., Pesquera, M., Fernie, A.R., Weber, A.P.M., and Fitzpatrick, T.B. (2016). Balancing of B-6 vitamers is essential for plant development and metabolism in Arabidopsis. Plant Cell 28:439-453.

Colon-Carmona, A., You, R., Haimovitch-Gal, T., and Doerner, P. (1999). Spatio-temporal analysis of mitotic activity with a labile cyclin-GUS fusion protein. Plant J 20:503-508.

Cruz, C., Bio, A.F.M., Dominguez-Valdivia, M.D., Aparicio-Tejo, P.M., Lamsfus, C., and Martins-Loucao, M.A. (2006). How does glutamine synthetase activity determine plant tolerance to ammonium? Planta 223:1068-1080.

Danon, A., Miersch, O., Felix, G., Camp, R.G., and Apel, K. (2005). Concurrent activation of cell death-regulating signaling pathways by singlet oxygen in Arabidopsis thaliana. Plant J 41:68-80.

Dell'Aglio, E., Boycheva, S., and Fitzpatrick, T.B. (2017). The Pseudoenzyme PDX1.2 Sustains Vitamin B-6 Biosynthesis as a Function of Heat Stress. Plant Physiol 174:2098-2112.

Dello Ioio, R., Linhares, F.S., Scacchi, E., Casamitjana-Martinez, E., Heidstra, R., Costantino, P., and Sabatini, S. (2007). Cytokinins determine Arabidopsis root-meristem size by controlling cell differentiation. Current Biology 17:678-682.

Dello Ioio, R., Nakamura, K., Moubayidin, L., Perilli, S., Taniguchi, M., Morita, M.T., Aoyama, T., Costantino, P., and Sabatini, S. (2008). A genetic framework for the control of cell division and differentiation in the root meristem. Science 322:1380-1384.

Dixon, S.J., and Stockwell, B.R. (2014). The role of iron and reactive oxygen species in cell death. Nat Chem Biol 10:9-17.

Dong, Q., Bai, B., Almutairi, B.O., and Kudla, J. (2021). Emerging roles of the CBL-CIPK calcium signaling network as key regulatory hub in plant nutrition. J Plant Physiol 257:153335.

Duan, F., Giehl, R.F.H., Geldner, N., Salt, D.E., and von Wirén, N. (2018). Root zone-specific localization of AMTs determines ammonium transport pathways and nitrogen allocation to shoots. PLoS Biol 16:e2006024.

Ferreira, F.J., and Kieber, J.J. (2005). Cytokinin signaling. Curr Opin Plant Biol 8:518-525.

Fitzpatrick, T.B. (2011). Vitamin B6 in plants: more than meets the eye. Adv Bot Res 59:1-38.

Fitzpatrick, T.B., Amrhein, N., Kappes, B., Macheroux, P., Tews, I., and Raschle, T. (2007). Two independent routes of de novo vitamin B6 biosynthesis: not that different after all. Biochem J 407:1-13.

Gazzarrini, S., Lejay, L., Gojon, A., Ninnemann, O., Frommer, W.B., and von Wirén, N. (1999). Three functional transporters for constitutive, diurnally regulated, and starvation-induced uptake of ammonium into arabidopsis roots. Plant Cell 11:937-947.

Gjetting, K.S.K., Ytting, C.K., Schulz, A., and Fuglsang, A.T. (2012). Live imaging of intra- and extracellular pH in plants using pHusion, a novel genetically encoded biosensor. J Exp Bot 63:3207-3218.

Green, L.S., and Rogers, E.E. (2004). FRD3 controls iron localization in Arabidopsis. Plant Physiol 136:2523-2531.

Guan, M., de Bang, T.C., Pedersen, C., and Schjoerring, J.K. (2016). Cytosolic glutamine synthetase Gln1;2 is the main isozyme contributing to GS1 activity and can be up-regulated to relieve ammonium toxicity. Plant Physiol 171:1921-1933.

Hachiya, T., Inaba, J., Wakazaki, M., Sato, M., Toyooka, K., Miyagi, A., Kawai-Yamada, M., Sugiura, D., Nakagawa, T., Kiba, T., et al. (2021). Excessive ammonium assimilation by plastidic glutamine synthetase causes ammonium toxicity in Arabidopsis thaliana. Nat Commun 12:4944.

Hangarter, R.P., and Stasinopoulos, T.C. (1991). Effect of Fe-catalyzed photooxidation of EDTA on root-growth in plant culture media. Plant Physiol 96:843-847.

Havaux, M., Ksas, B., Szewczyk, A., Rumeau, D., Franck, F., Caffarri, S., and Triantaphylides, C. (2009). Vitamin B6 deficient plants display increased sensitivity to high light and photo-oxidative stress. BMC Plant Biol 9.

Ishiyama, K., Inoue, E., Watanabe-Takahashi, A., Obara, M., Yamaya, T., and Takahashi, H. (2004). Kinetic properties and ammonium-dependent regulation

of cytosolic isoenzymes of glutamine synthetase in Arabidopsis. J Biol Chem 279:16598-16605.

Jain, S.K., and Lim, G. (2001). Pyridoxine and pyridoxamine inhibits superoxide radicals and prevents lipid peroxidation, protein glycosylation, and (Na^++K^+)-ATPase activity reduction in high glucose-treated human erythrocytes. Free Radical Bio Med 30:232-237.

Jian, S.F., Liao, Q., Song, H.X., Liu, Q., Lepo, J.E., Guan, C.Y., Zhang, J.H., Ismail, A.M., and Zhang, Z.H. (2018). NRT1.1-related NH_4^+ toxicity is associated with a disturbed balance between NH_4^+ uptake and assimilation. Plant Physiol 178:1473-1488.

Jiang, C.F., Belfield, E.J., Mithani, A., Visscher, A., Ragoussis, J., Mott, R., Smith, J.A.C., and Harberd, N.P. (2012). ROS-mediated vascular homeostatic control of root-to-shoot soil Na delivery in Arabidopsis. Embo J 31:4359-4370.

Ju, X.T., Xing, G.X., Chen, X.P., Zhang, S.L., Zhang, L.J., Liu, X.J., Cui, Z.L., Yin, B., Christie, P., Zhu, Z.L., et al. (2009). Reducing environmental risk by improving N management in intensive Chinese agricultural systems. P Natl Acad Sci USA 106:3041-3046.

Kannan, K., and Jain, S.K. (2004). Effect of vitamin B-6 on oxygen radicals, mitochondrial membrane potential, and lipid peroxidation in H_2O_2-treated U937 monocytes. Free Radical Bio Med 36:423-428.

Kehrer, J.P. (2000). The Haber-Weiss reaction and mechanisms of toxicity. Toxicology 149:43-50.

Kempinski, C.F., Haffar, R., and Barth, C. (2011). Toward the mechanism of NH_4^+ sensitivity mediated by Arabidopsis GDP-mannose pyrophosphorylase. Plant Cell Environ 34:847-858.

Khan, A.U., and Kasha, M. (1994). Singlet molecular-oxygen in the Haber-Weiss reaction. P Natl Acad Sci USA 91:12365-12367.

Konishi, N., Ishiyama, K., Beier, M.P., Inoue, E., Kanno, K., Yamaya, T., Takahashi, H., and Kojima, S. (2017). Contributions of two cytosolic glutamine synthetase isozymes to ammonium assimilation in Arabidopsis roots. J Exp Bot 68:613-625.

Koppenol, W.H., and Hider, R.H. (2019). Iron and redox cycling. Do's and don'ts. Free radical biology & medicine 133:3-10.

Lager, I., Andreasson, O., Dunbar, T.L., Andreasson, E., Escobar, M.A., and Rasmusson, A.G. (2010). Changes in external pH rapidly alter plant gene expression and modulate auxin and elicitor responses. Plant Cell Environ 33:1513-1528.

Lee, Y., Rubio, M.C., Alassimone, J., and Geldner, N. (2013). A mechanism for localized lignin deposition in the endodermis. Cell 153:402-412.

Leskovi, A., Zvari, K.M., Araya, T., and Giehl, R.F.H. (2020). Nickel toxicity targets cell wall-related processes and PIN2-mediated auxin transport to inhibit root elongation and gravitropic responses in Arabidopsis. Plant Cell Physiol 61:519-535.

Li, B.H., Li, G.J., Kronzucker, H.J., Baluska, F., and Shi, W.M. (2014). Ammonium stress in Arabidopsis: signaling, genetic loci, and physiological targets. Trends in plant science 19:107-114.

Li, G., Zhang, L., Wang, M., Di, D., Kronzucker, H.J., and Shi, W. (2019). The Arabidopsis AMOT1/EIN3 gene plays an important role in the amelioration of ammonium toxicity. J Exp Bot 70:1375-1388.

Li, Q., Li, B.H., Kronzucker, H.J., and Shi, W.M. (2010). Root growth inhibition by NH_4^+ in Arabidopsis is mediated by the root tip and is linked to NH_4^+ efflux and GMPase activity. Plant Cell Environ 33:1529-1542.

Li, X. (2011). Histostaining for tissue expression pattern of promoter-driven GUS activity in Arabidopsis. Bio-101 e93.

Lima, J.E., Kojima, S., Takahashi, H., and von Wirén, N. (2010). Ammonium triggers lateral root branching in Arabidopsis in an AMMONIUM TRANSPORTER1;3-dependent manner. Plant Cell 22:3621-3633.

Liu, Y., Lai, N., Gao, K., Chen, F., Yuan, L., and Mi, G. (2013). Ammonium inhibits primary root growth by reducing the length of meristem and elongation zone and decreasing elemental expansion rate in the root apex in Arabidopsis thaliana. Plos One 8:e61031.

Liu, Y., and von Wiren, N. (2017). Ammonium as a signal for physiological and morphological responses in plants. J Exp Bot 68:2581-2592.

Loque, D., Ludewig, U., Yuan, L., and von Wiren, N. (2005). Tonoplast intrinsic proteins AtTIP2;1 and AtTIP2;3 facilitate NH_3 transport into the vacuole. Plant Physiol 137:671-680.

Lothier, J., Gaufichon, L., Sormani, R., Lemaitre, T., Azzopardi, M., Morin, H., Chardon, F., Reisdorf-Cren, M., Avice, J.C., and Masclaux-Daubresse, C. (2011). The cytosolic glutamine synthetase GLN1;2 plays a role in the control of plant growth and ammonium homeostasis in Arabidopsis rosettes when nitrate supply is not limiting. J Exp Bot 62:1375-1390.

Mahfouz, M.M., Zhou, S.Q., and Kummerow, F.A. (2009). Vitamin B6 compounds are capable of reducing the superoxide radical and lipid peroxide levels induced by H_2O_2 in vascular endothelial cells in culture. Int J Vitam Nutr Res 79:218-229.

Meier, M., Liu, Y., Lay-Pruitt, K.S., Takahashi, H., and von Wirén, N. (2020). Auxin-mediated root branching is determined by the form of available nitrogen. Nat Plants 6:1136-1145.

Moccand, C., Boycheva, S., Surriabre, P., Tambasco-Studart, M., Raschke, M., Kaufmann, M., and Fitzpatrick, T.B. (2014). The pseudoenzyme PDX1.2 boosts vitamin B-6 biosynthesis under heat and oxidative stress in Arabidopsis. J Biol Chem 289:8203-8216.

Mooney, S., and Hellmann, H. (2010). Vitamin B6: Killing two birds with one stone? Phytochemistry 71:495-501.

Mora-Macias, J., Ojeda-Rivera, J.O., Gutierrez-Alanis, D., Yong-Villalobos, L., Oropeza-Aburto, A., Raya-Gonzalez, J., Jimenez-Dominguez, G., Chavez-Calvillo, G., Rellan-Alvarez, R., and Herrera-Estrella, L. (2017). Malate-dependent Fe accumulation is a critical checkpoint in the root developmental response to low phosphate. P Natl Acad Sci USA 114:E3563-E3572.

Muller, J., Toev, T., Heisters, M., Teller, J., Moore, K.L., Hause, G., Dinesh, D.C., Burstenbinder, K., and Abel, S. (2015). Iron-dependent callose deposition adjusts root meristem maintenance to phosphate availability. Dev Cell 33:216-230.

Nakayama, S., Sugano, S.S., Hirokawa, H., Mori, I.C., Daimon, H., Kimura, S., and Fukao, Y. (2020). Manganese treatment alleviates zinc deficiency symptoms in Arabidopsis seedlings. Plant Cell Physiol 61:1711-1723.

Nkebiwe, P.M., Weinmann, M., Bar-Tal, A., and Muller, T. (2016). Fertilizer placement to improve crop nutrient acquisition and yield: A review and meta-analysis. Field Crop Res 196:389-401.

Patterson, K., Cakmak, T., Cooper, A., Lager, I., Rasmusson, A.G., and Escobar, M.A. (2010). Distinct signalling pathways and transcriptome response signatures differentiate ammonium- and nitrate-supplied plants. Plant Cell Environ 33:1486-1501.

Percudani, R., and Peracchi, A. (2003). A genomic overview of pyridoxal-phosphate-dependent enzymes. Embo Rep 4:850-854.

Qin, C., Qian, W.Q., Wang, W.F., Wu, Y., Yu, C.M., Jiang, X.H., Wang, D.W., and Wu, P. (2008). GDP-mannose pyrophosphorylase is a genetic determinant of ammonium sensitivity in Arabidopsis thaliana. P Natl Acad Sci USA 105:18308-18313.

Ragel, P., Rodenas, R., Garcia-Martin, E., Andres, Z., Villalta, I., Nieves-Cordones, M., Rivero, R.M., Martinez, V., Pardo, J.M., Quintero, F.J., et al. (2015). The CBL-interacting protein kinase CIPK23 regulates HAK5-mediated high-affinity K^+ uptake in Arabidopsis roots. Plant Physiol 169:2863-2873.

Raschke, M., Boycheva, S., Crevecoeur, M., Nunes-Nesi, A., Witt, S., Fernie, A.R., Amrhein, N., and Fitzpatrick, T.B. (2011). Enhanced levels of vitamin B-6 increase aerial organ size and positively affect stress tolerance in Arabidopsis. Plant J 66:414-432.

Raschle, T., Arigoni, D., Brunisholz, R., Rechsteiner, H., Amrhein, N., and Fitzpatrick, T.B. (2007). Reaction mechanism of pyridoxal 5 '-phosphate synthase - Detection of an enzyme-bound chromophoric intermediate. J Biol Chem 282:6098-6105.

Ristova, D., Carre, C., Pervent, M., Medici, A., Kim, G.J., Scalia, D., Ruffel, S., Birnbaum, K.D., Lacombe, B., Busch, W., et al. (2016). Combinatorial interaction network of transcriptomic and phenotypic responses to nitrogen and hormones in the Arabidopsis thaliana root. Science signaling 9:rs13.

Rogato, A., D'Apuzzo, E., Barbulova, A., Omrane, S., Parlati, A., Carfagna, S., Costa, A., Lo Schiavo, F., Esposito, S., and Chiurazzi, M. (2010). Characterization of a developmental root response caused by external ammonium supply in Lotus japonicus. Plant Physiol 154:784-795.

Romheld, V., and Marschner, H. (1986). Evidence for a specific uptake system for iron phytosiderophores in roots of grasses. Plant Physiol 80:175-180.

Roschzttardtz, H., Conejero, G., Curie, C., and Mari, S. (2009). Identification of the endodermal vacuole as the iron storage compartment in the Arabidopsis embryo. Plant Physiol 151:1329-1338.

Sanchez-Barrena, M.J., Chaves-Sanjuan, A., Raddatz, N., Mendoza, I., Cortes, A., Gago, F., Gonzalez-Rubio, J.M., Benavente, J.L., Quintero, F.J., Pardo, J.M., et al. (2020). Recognition and activation of the plant AKT1 potassium channel by the kinase CIPK23. Plant Physiol 182:2143-2153.

Shi, S.J., Xu, F.Z., Ge, Y.Q., Mao, J.J., An, L.L., Deng, S.J., Ullah, Z., Yuan, X.F., Liu, G.S., Liu, H.B., et al. (2020). NH_4^+ toxicity, which is mainly determined by the high NH_4^+/K^+ ratio, is alleviated by CIPK23 in Arabidopsis. Plants 9.

Smirnoff, N., and Arnaud, D. (2018). Hydrogen peroxide metabolism and functions in plants. New Phytol 221:1197-1214.

Stolz, J., and Vielreicher, M. (2003). Tpn1p, the plasma membrane vitamin B_6 transporter of Saccharomyces cerevisiae. J Biol Chem 278:18990-18996.

Straub, T., Ludewig, U., and Neuhaeuser, B. (2017). The kinase CIPK23 inhibits ammonium transport in *Arabidopsis thaliana*. Plant Cell 29:409-422.

Sun, L., Di, D.W., Li, G.J., Kronzucker, H.J., Wu, X.Y., and Shi, W.M. (2020). Endogenous ABA alleviates rice ammonium toxicity by reducing ROS and free

ammonium via regulation of the SAPK9-bZIP20 pathway. J Exp Bot 71:4562-4577.

Sutton, M.A., Oenema, O., Erisman, J.W., Leip, A., van Grinsven, H., and Winiwarter, W. (2011). Too much of a good thing. Nature 472:159-161.

Szydlowski, N., Burkle, L., Pourcel, L., Moulin, M., Stolz, J., and Fitzpatrick, T.B. (2013). Recycling of pyridoxine (vitamin B_6) by PUP1 in Arabidopsis. Plant J 75:40-52.

Tambasco-Studart, M., Titiz, O., Raschle, T., Forster, G., Amrhein, N., and Fitzpatrick, T.B. (2005). Vitamin B6 biosynthesis in higher plants. P Natl Acad Sci USA 102:13687-13692.

Thordal-Christensen, H., Zhang, Z.G., Wei, Y.D., and Collinge, D.B. (1997). Subcellular localization of H_2O_2 in plants. H_2O_2 accumulation in papillae and hypersensitive response during the barley-powdery mildew interaction. Plant J 11:1187-1194.

Tian, Q., Uhlir, N.J., and Reed, J.W. (2002). Arabidopsis SHY2/IAA3 inhibits auxin-regulated gene expression. Plant Cell 14:301-319.

Titiz, O., Tambasco-Studart, M., Warzych, E., Apel, K., Amrhein, N., Laloi, C., and Fitzpatrick, T.B. (2006). PDX1 is essential for vitamin B6 biosynthesis, development and stress tolerance in Arabidopsis. Plant J 48:933-946.

Tsukagoshi, H. (2016). Control of root growth and development by reactive oxygen species. Curr Opin Plant Biol 29:57-63.

Tsukagoshi, H., Busch, W., and Benfey, P.N. (2010). Transcriptional Regulation of ROS Controls Transition from Proliferation to Differentiation in the Root. Cell 143:606-616.

Vandesompele, J., De Preter, K., Pattyn, F., Poppe, B., Van Roy, N., De Paepe, A., and Speleman, F. (2002). Accurate normalization of real-time quantitative RT-PCR data by geometric averaging of multiple internal control genes. Genome Biol 3.

Wagner, S., Bernhardt, A., Leuendorf, J.E., Drewke, C., Lytovchenko, A., Mujahed, N., Gurgui, C., Frommer, W.B., Leistner, E., Fernie, A.R., et al. (2006). Analysis of the Arabidopsis rsr4-1/pdx1-3 mutant reveals the critical function of the PDX1 protein family in metabolism, development, and vitamin B6 biosynthesis. Plant Cell 18:1722-1735.

Wasil, M., Halliwell, B., Grootveld, M., Moorhouse, C.P., Hutchison, D.C., and Baum, H. (1987). The specificity of thiourea, dimethylthiourea and dimethyl sulphoxide as scavengers of hydroxyl radicals. Their protection of alpha 1-antiproteinase against inactivation by hypochlorous acid. Biochem J 243:867-870.

Watt, M., Silk, W.K., and Passioura, J.B. (2006). Rates of root and organism growth, soil conditions, and temporal and spatial development of the rhizosphere. Ann Bot-London 97:839-855.

Xie, Y.J., Mao, Y., Xu, S., Zhou, H., Duan, X.L., Cui, W.T., Zhang, J., and Xu, G.H. (2015). Heme-heme oxygenase 1 system is involved in ammonium tolerance by regulating antioxidant defence in Oryza sativa. Plant Cell Environ 38:129-143.

Xu, G.H., Fan, X.R., and Miller, A.J. (2012). Plant nitrogen assimilation and use efficiency. Annual Review of Plant Biology 63:153-182.

Zheng, Z., Wang, Z., Wang, X.Y., and Liu, D. (2019). Blue light-triggered chemical reactions underlie phosphate deficiency-induced inhibition of root elongation of Arabidopsis seedlings grown in Petri dishes. Mol Plant 12:1515-1523.

Journal Pre-proof

Zhu, C.Q., Zhang, J.H., Zhu, L.F., Abliz, B., Zhong, C., Bai, Z.G., Hu, W.J., Sajid, H., James, A.B., Cao, X.C., et al. (2018). NH_4^+ facilitates iron reutilization in the cell walls of rice (Oryza sativa) roots under iron-deficiency conditions. Environ Exp Bot 151:21-31.

Journal Pre-proof

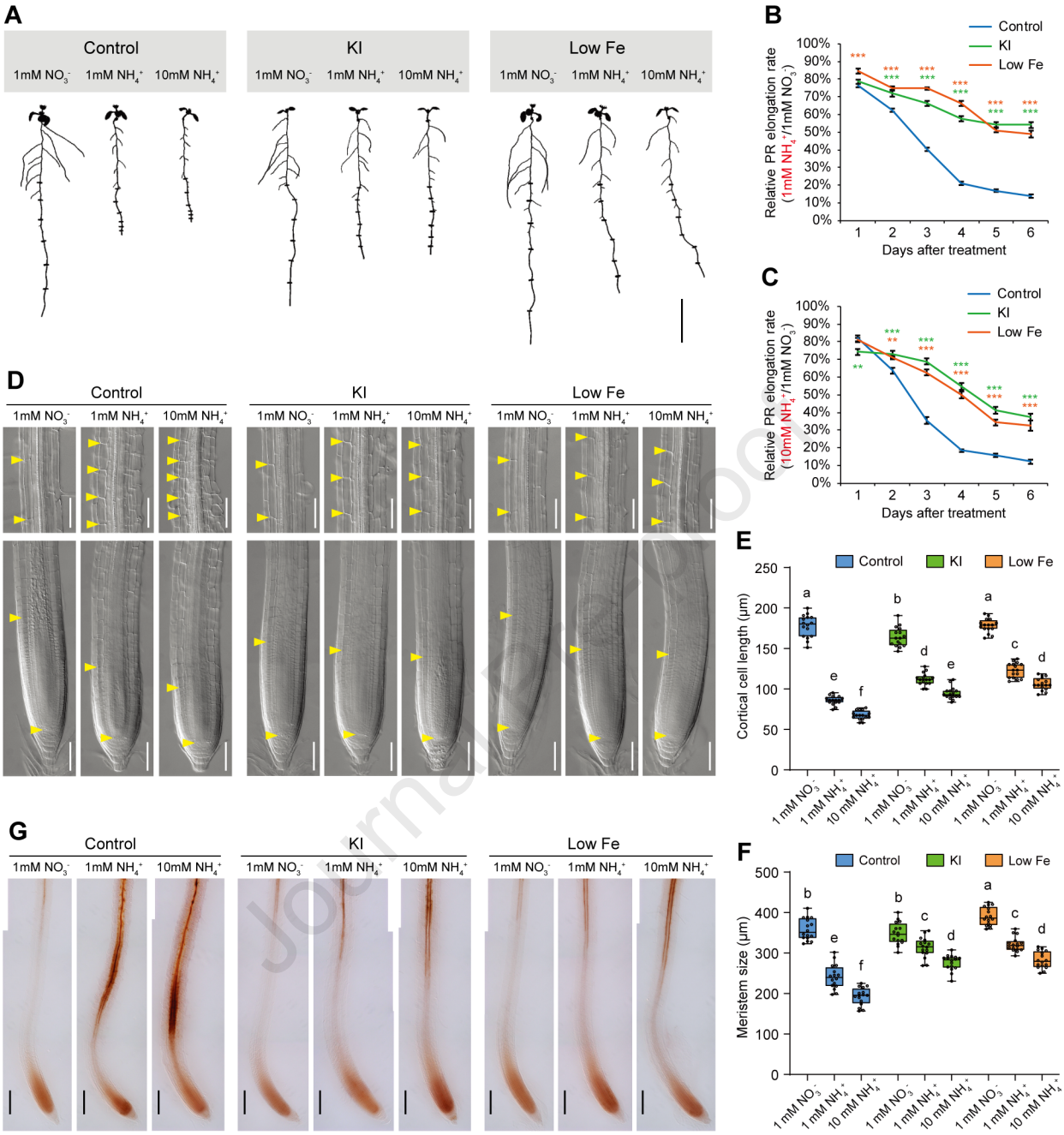

Journal Pre-proof

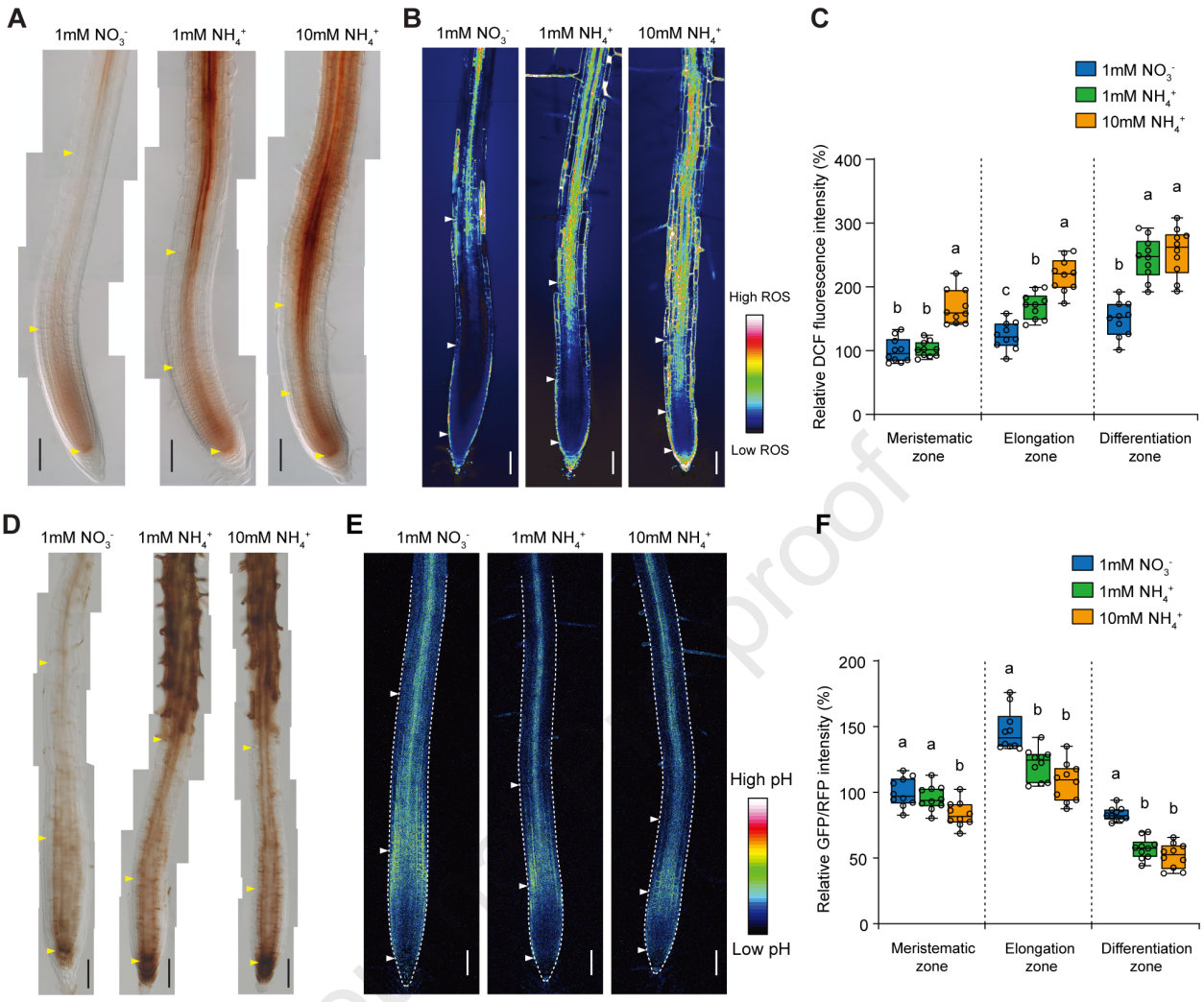
A
1mM NO3-
1mM NH4+
10mM NH4+
B
1mM NO3-
1mM NH4+
10mM NH4+
High ROS
Low ROS
C
1mM NO3-
1mM NH4+
10mM NH4+
Relative DCF fluorescence intensity (%)
0
100
200
300
400
b
b
a
c
b
a
b
a
a
Meristematic zone
Elongation zone
Differentiation zone
D
1mM NO3-
1mM NH4+
10mM NH4+
E
1mM NO3-
1mM NH4+
10mM NH4+
High pH
Low pH
F
1mM NO3-
1mM NH4+
10mM NH4+
Relative GFP/RFP intensity (%)
0
50
100
150
200
a
a
b
a
b
b
a
b
b
Meristematic zone
Elongation zone
Differentiation zone

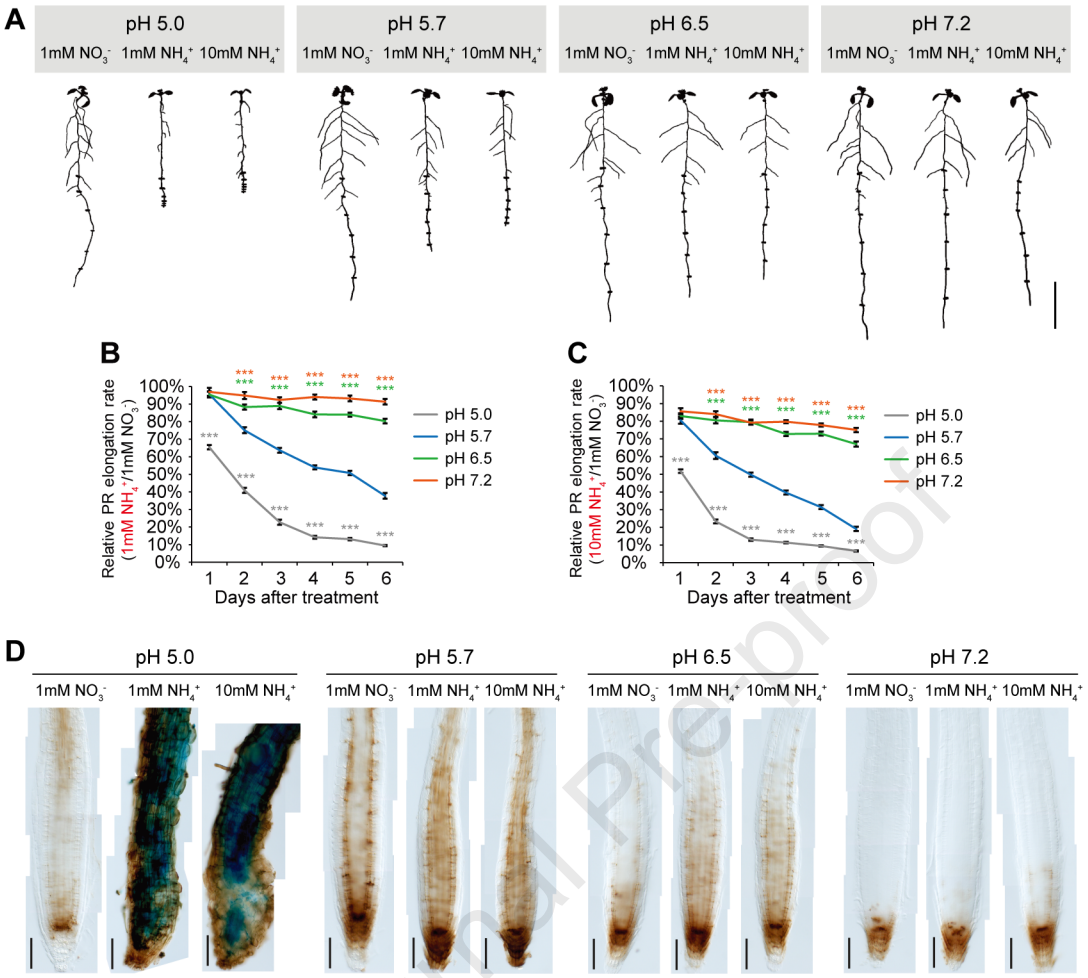

Journal Pre-proof

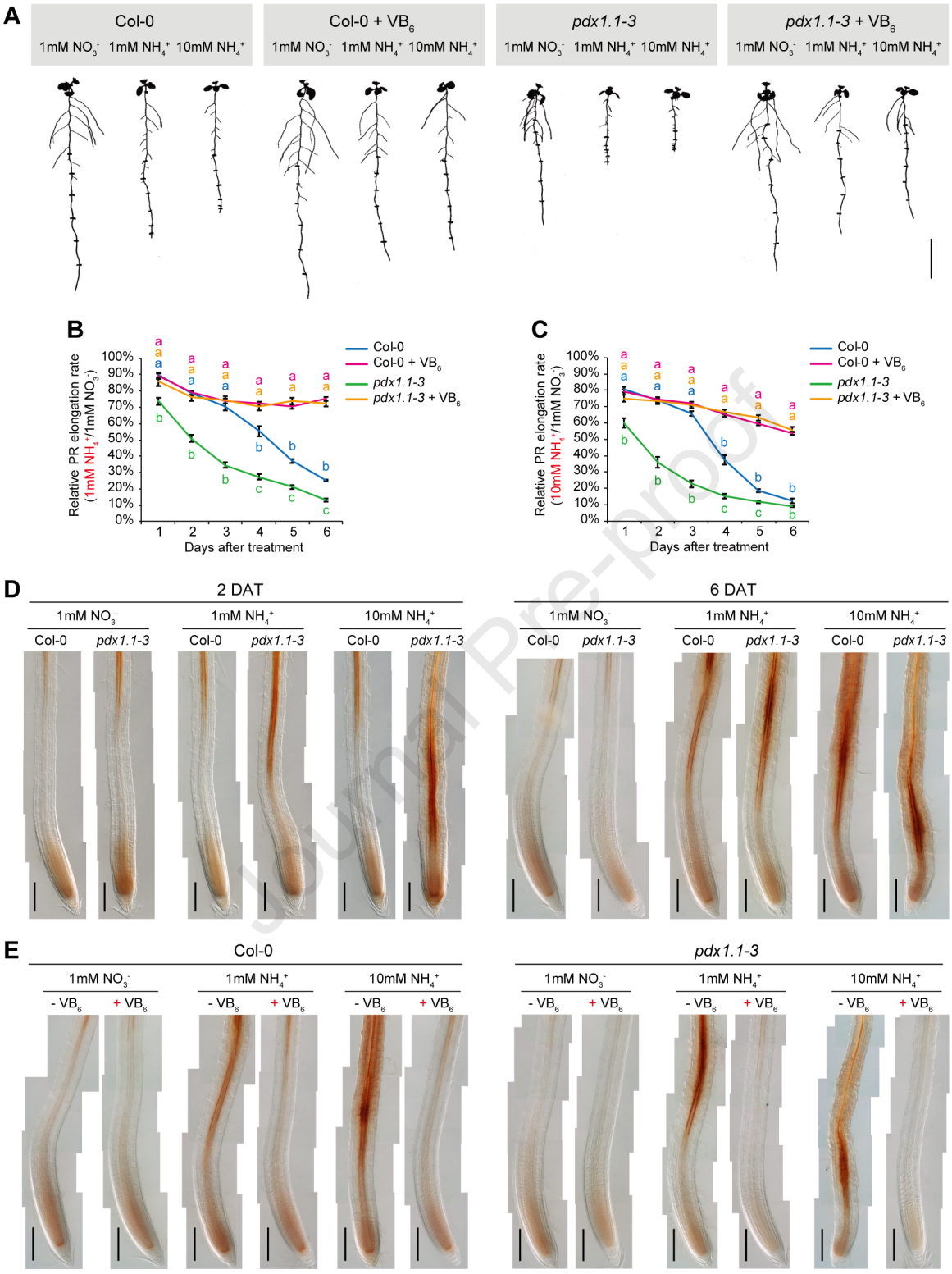

Journal Pre-proof

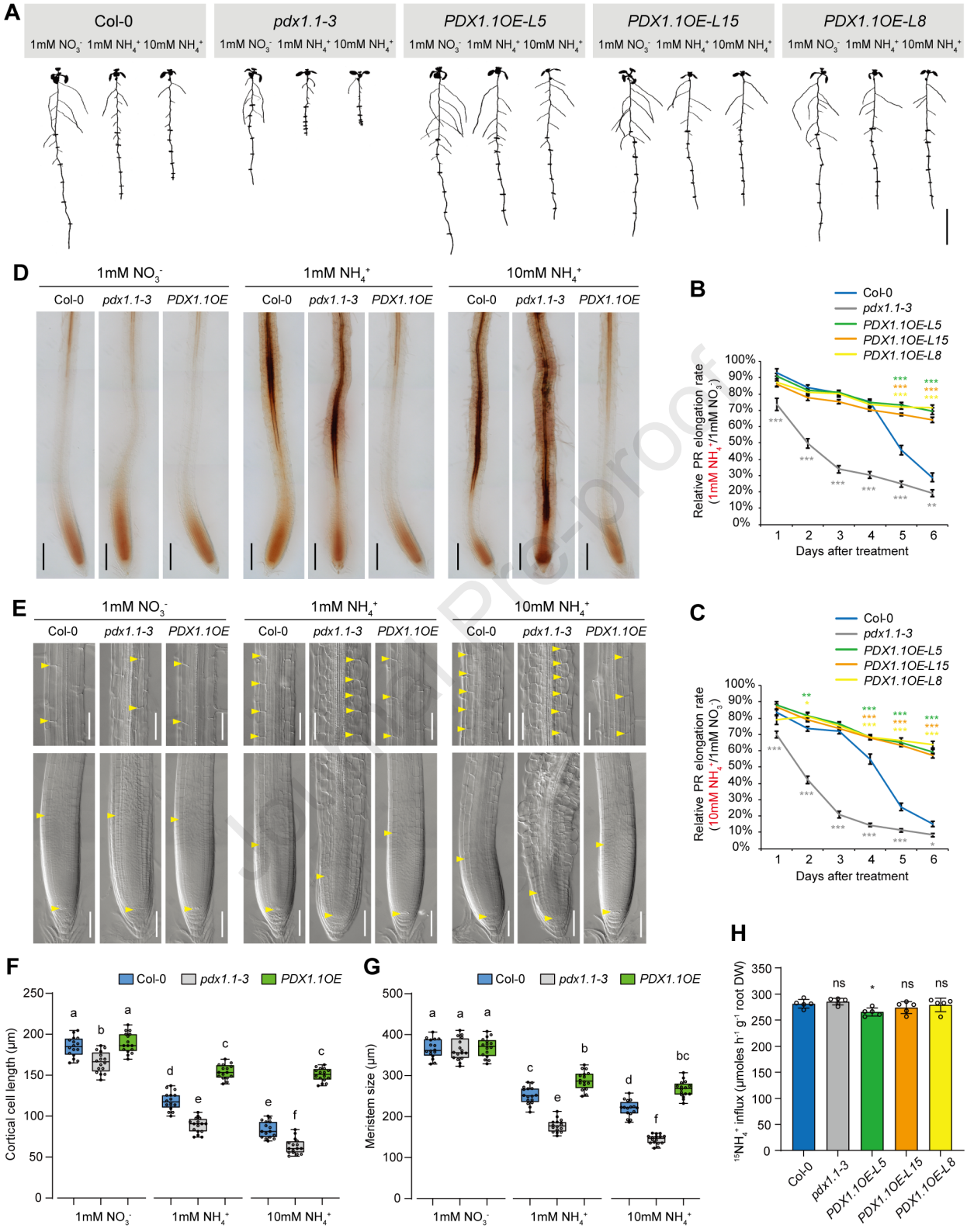
A
Col-0
pdx1.1-3
PDX1.1OE-L5
PDX1.1OE-L15
PDX1.1OE-L8
1mM NO3- 1mM NH4+ 10mM NH4+
D
1mM NO3-
1mM NH4+
10mM NH4+
Col-0
pdx1.1-3
PDX1.1OE
B
Col-0
pdx1.1-3
PDX1.1OE-L5
PDX1.1OE-L15
PDX1.1OE-L8
Relative PR elongation rate (1mM NH4+/1mM NO3-)
Days after treatment
E
C
Relative PR elongation rate (10mM NH4+/1mM NO3-)
F
Cortical cell length (μm)
G
Meristem size (μm)
H
15NH4+ influx (μmoles h-1 g-1 root DW)
ns
*

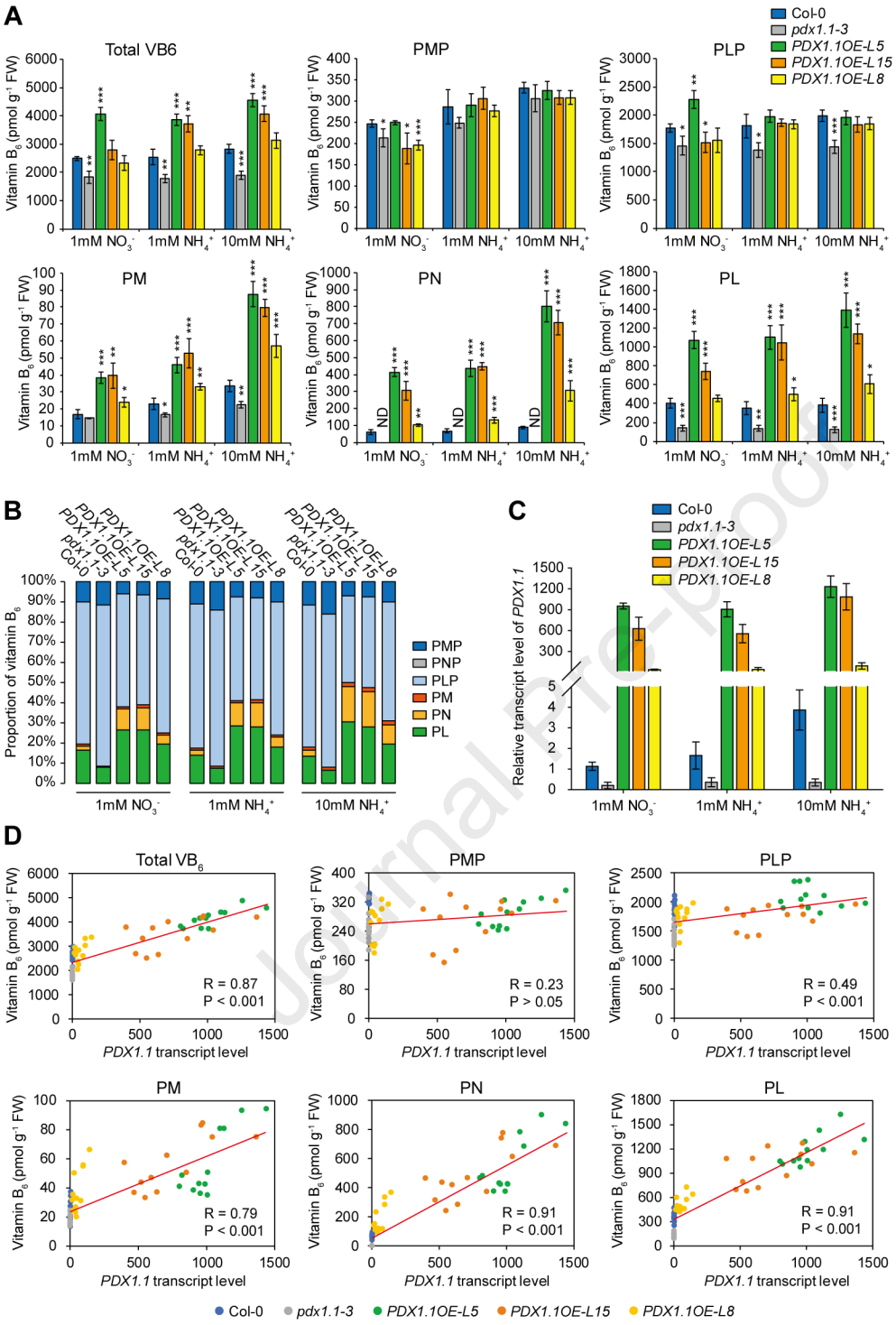

Journal Pre-proof

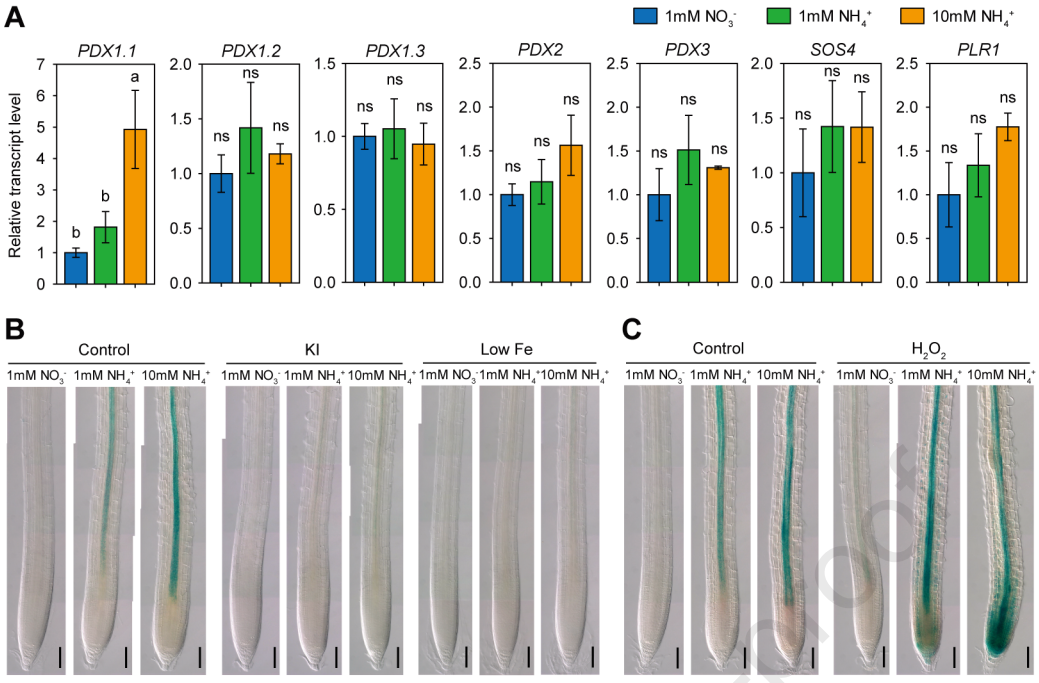
A
1mM NO3-
1mM NH4+
10mM NH4+
PDX1.1
PDX1.2
PDX1.3
PDX2
PDX3
SOS4
PLR1
Relative transcript level
B
Control
KI
Low Fe
C
Control
H2O2

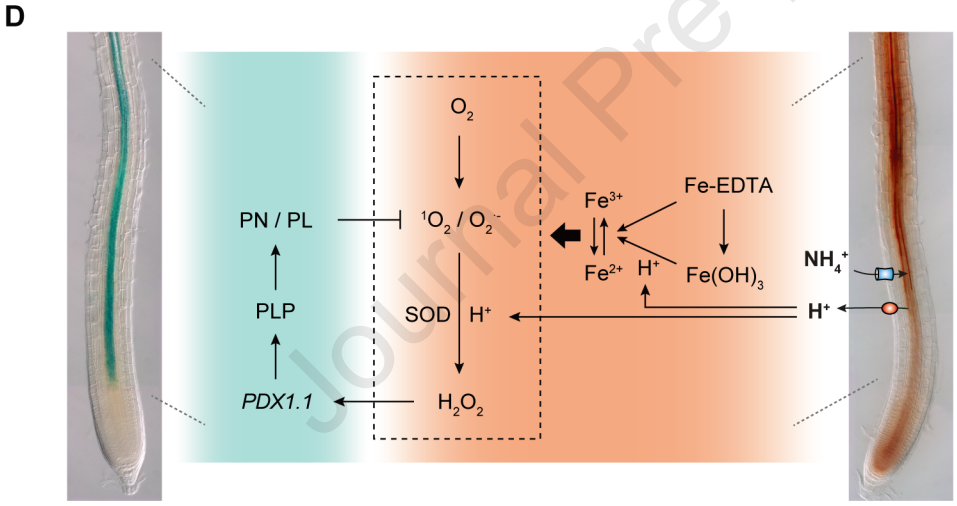
D
O2
PN / PL
1O2 / O2-
Fe3+
Fe-EDTA
Fe2+
H+
Fe(OH)3
NH4+
PLP
SOD
H+
PDX1.1
H2O2